Author Query Form

Journal: FEBS

Article: 70389

Dear Author,

During the copyediting of your manuscript the following queries arose.

Please refer to the query reference callout numbers in the page proofs and respond.

Please remember illegible or unclear comments and corrections may delay publication.

Many thanks for your assistance.

AUTHOR: Please note that missing content in references have been updated where we have been able to match the missing elements without ambiguity against a standard citation database, to meet the reference style requirements of the journal. It is your responsibility to check and ensure that all listed references are complete and accurate.

Query reference	Query	Remarks
1	**AUTHOR: Please check all website addresses and the functionality of the underlying links and confirm that they are correct. (Please note that it is the responsibility of the author(s) to ensure that all URLs given in this article are correct and usable.)**	
2	**AUTHOR: Please suggest whether the term 'anti-malarial' can be changed to 'antimalarial' in the article title.**	
3	**AUTHOR: Please check and confirm that the graphical abstract is fine for publication.**	
4	**AUTHOR: Please check if Figure 1 has been reproduced from Ref. [32]. Please add the statement "Figure reproduced from Ref. [32]" to the end of figure caption if Figure 1 has been reproduced from published sources. Please also confirm if written permission has been obtained from the publisher/author if Figure 1 has been reproduced. Please ignore this query if figure parts described as being modified from other publications are sufficiently different and do not require permission statements for reproduction from the previous publisher/author. Please indicate in the query sheet as "Ignore" if this author query can be ignored.**	

5	**AUTHOR: Please check if Figure 2 has been reproduced from Ref. [45, 46]. Please add the statement "Figure reproduced from Ref. [45, 46]" to the end of figure caption if Figure 2 has been reproduced from published sources. Please also confirm if written permission has been obtained from the publisher/author if Figure 2 has been reproduced. Please ignore this query if figure parts described as being modified from other publications are sufficiently different and do not require permission statements for reproduction from the previous publisher/author. Please indicate in the query sheet as "Ignore" if this author query can be ignored.**	
6	**AUTHOR: Please cite footnote "a" in Table [1].**	
7	**AUTHOR: Please check if Figure 3 has been reproduced from Ref. [9, 24, 26, 47]. Please add the statement "Figure reproduced from Ref. [9, 24, 26, 47]" to the end of figure caption if Figure 3 has been reproduced from published sources. Please also confirm if written permission has been obtained from the publisher/author if Figure 3 has been reproduced. Please ignore this query if figure parts described as being modified from other publications are sufficiently different and do not require permission statements for reproduction from the previous publisher/author. Please indicate in the query sheet as "Ignore" if this author query can be ignored.**	
8	**AUTHOR: Please check if Figure 4 has been reproduced from Ref. [22, 46]. Please add the statement "Figure reproduced from Ref. [22, 46]" to the end of figure caption if Figure 4 has been reproduced from published sources. Please also confirm if written permission has been obtained from the publisher/author if Figure 4 has been reproduced. Please ignore this query if figure parts described as being modified from other publications are sufficiently different and do not require permission statements for reproduction from the previous publisher/author. Please indicate in the query sheet as "Ignore" if this author query can be ignored.**	
9	**AUTHOR: Please check if Figure 5 has been reproduced from Ref. [24, 27, 46]. Please add the statement "Figure reproduced from Ref. [24, 27, 46]" to the end of figure caption if Figure 5 has been reproduced from published sources. Please also confirm if written permission has been obtained from the publisher/author if Figure 5 has been reproduced. Please ignore this query if figure parts described as being modified from other publications are sufficiently different and do not require permission statements for reproduction from the previous publisher/author. Please indicate in the query sheet as "Ignore" if this author query can be ignored.**	
10	**AUTHOR: Please check if Figure 10 has been reproduced from Ref. [23, 47]. Please add the statement "Figure reproduced from Ref. [23, 47]" to the end of figure caption if Figure 10 has been reproduced from published sources. Please also confirm if written permission has been obtained from the publisher/author if Figure 10 has been reproduced. Please ignore this query if figure parts described as being modified from other publications are sufficiently different and do not require permission statements for reproduction from the previous publisher/author. Please indicate in the query sheet as "Ignore" if this author query can be ignored.**	
11	**AUTHOR: Please give address information for this Greiner Bio-One, Douglas Instruments, Neobiotech, Millipore, Constant Systems Ltd., Novagen, Clontech, Thermo Fisher Scientific, Bio-Rad, Promega, New England Biolabs: town, state (if applicable), and country.**	
12	**AUTHOR: Reference numbers have been reordered to appear sequentially. Please check and confirm this was done correctly.**	

The FEBS Journal

FEBS PRESS science publishing by scientists

Targeting the histone-fold dimerization interface of oocyst rupture proteins from *Plasmodium berghei* for anti-malarial inhibitor discovery

Federico Ballabio[1,2,*], Chiara Bertaso[1], Marta Villa[1], Ophelia Livero[1,†], Alessandro Del Cont Bernard[1,‡], Rosaria Russo[3], Renate Gessmann[4], Inga Siden-Kiamos[4], Claude Marie Francois Preira[5], Amit Kumawat[1,¶], Paolo Gabrieli[1], Carlo Camilloni[1], Chiara Currà[4,6], Simona Masiero[1], Marco Nardini[1] and Louise J. Gourlay[1]

1 Department of Biosciences, University of Milano, Italy
2 National Research Council of Italy, Biophysics Institute (CNR-IBF), Milan, Italy
3 Department of Pathophysiology and Transplantation, L.I.T.A. Segrate, Italy
4 Foundation for Research and Technology Hellas, Institute of Molecular biology and Biotechnology, Heraklion, Crete, Greece
5 Department of Biology, Voutes University Campus, University of Crete, Heraklion, Crete, Greece
6 Department of Infectious Diseases, Istituto Superiore di Sanità, Rome, Italy

Keywords
cyclic peptide inhibitors; histone-fold domain; *in silico* molecular docking; oocyst rupture proteins; *Plasmodium* spp.

Correspondence
L. J. Gourlay, Department of Biosciences, University of Milano, Via Celoria 26, Milan, Italy
Tel: +39 (0)2 50314903
E-mail: louise.gourlay@unimi.it
Website: https://dbs.unimi.it/it

Present address
*Institute of Structural Biology, Molecular Targets and Therapeutics Center, Helmholtz Munich – Deutsches Forschungszentrum Für Gesundheit Und Umwelt (GmbH), Neuherberg, Germany
†European Brain Research Institute Rita Levi-Montalcini, Rome, Italy
‡European Synchrotron Radiation Facility, Grenoble, France
¶Department of Physics, Università degli Studi di Cagliari, Monserrato, Italy

Federico Ballabio, Chiara Bertaso and Marta Villa contributed equally to the work.

Dimerization between the histone-fold domains (HFD) of two *Plasmodium* Oocyst Rupture Proteins (ORP1 and ORP2) is essential for oocyst rupture in the *Anopheles* mosquito vector host, representing a key event in parasite transmission to humans. Notably, ORPs are a rare example of HFD-containing proteins that operate outside the nucleus and that lack DNA-binding functions, typically associated with core histones and transcription factors hosting deviant histones. ORP HFD heterodimerization occurs at the outer capsule of the oocyst, immediately prior to rupture, thus providing a temporal window to administer dimerization blocking molecules. In this context, we present the first detailed structural analysis of the HFD ORP heterodimer, solved by X-ray crystallography at 3.1 Å resolution, and analyze the oligomerization interface as a possible druggable target. Targeting the mosquito phase of the parasite lifecycle remains an under-exploited avenue as present antimalarial therapies mainly target the human blood stages of infection. We employed a GAL4-based yeast two-hybrid (Y2H) combinatorial library of cyclic peptides (CPs) to identify six candidates that inhibit dimerization *in vitro*. Molecular docking simulations confirmed that all six CPs bind at the dimer interface, allowing us to rank them for further *in vivo* testing of their efficacy in blocking oocyst rupture.

Abbreviations
AD, Gal4 activation domain; ATSB, attractive targeted sugar bait; CP, cyclic peptide; DBD, Gal4 DNA-binding domain; HFD, histone-fold domain; mAU, milli-absorbance unit; MW, molecular weight; NF-Y, nuclear factor Y; OD, optical density; ORP, oocyst rupture protein; PDB, protein data bank; RMSD, root mean square deviation; SEC, size exclusion chromatography; Sos, Son-of-sevenless; V_e, elution volume; Y2H, yeast two-hybrid.

(Received 24 June 2025, revised 7 October 2025, accepted 24 December 2025)

doi:10.1111/febs.70389

Introduction

Malaria, a well-known mosquito-borne disease caused by the *Plasmodium* parasite, continues to weigh a heavy burden on human morbidity and mortality on a global scale, with an estimated 263 million malaria cases and 597 000 malaria deaths worldwide in 2024 (World Malaria Report 2024) [1]. Currently, the recommended antimalarial drugs of choice are the fast-acting and well-tolerated artemesinin derivatives (e.g. dihydroartemisinin, artesunate, and artemether), typically administered in combination with partner drugs. However, emerging resistance to these therapies has been reported, underlining the urgent necessity to search for alternative antimalarial strategies [2].

In this context, we selected two oocyst rupture proteins (ORP1 and ORP2), expressed during the *Plasmodium* oocyst developmental stage, as potential novel antimalarial targets, given their critical roles in parasite transmission to humans [3,4]. Oocyst development occurs in the *Anopheles* mosquito vector and represents the longest stage in the parasite's life cycle, during which infective sporozoites are produced. Upon subsequent growth and rupture, sporozoites are released and migrate to the salivary glands where they inoculate and infect the human host when the mosquito takes its next blood meal. In the human host, sporozoites migrate to the liver where they mature into schizonts before eventually rupturing and releasing merozoites into the bloodstream [5]. After successive human blood developmental stages, including asexual multiplication, some parasites differentiate into gametocytes, which are ingested by the mosquito when it takes its next bite. In the mosquito, the sexual phase takes place leading to the formation of zygotes and subsequent motile ookinetes, which migrate to the mosquito midgut and develop into oocysts [5].

ORP1 is expressed during both the blood and mosquito stages of the *Plasmodium* life cycle, whereas ORP2 is only present in the mosquito stage. In the oocyst (also termed cyst) that develops in the mosquito midgut, ORP1 is located in the protective, outer capsule, whereas ORP2 is found inside the cyst, and at the periphery of the oocyst during maturation [4]. The capsule composition is poorly understood and except for the two ORPs, only three other capsule proteins have been reported [4,6–8]. Both *Plasmodium* ORP1 and ORP2 are large proteins consisting of 950 and 875 amino acids, respectively. They possess a single annotated domain in their primary structure, the histone-fold domain (HFD), characteristic of core histones and 'histone-like' proteins in eukaryotes and archaea [9–11]. In ORP1, the HFD is located at the C terminus ($ORP1^{HFD}$: residues 774–839; Pfam00808), whereas in ORP2, it is found at the N terminus ($ORP2^{HFD}$: residues 23–109; Pfam00125).

The 'canonical' HFD consists of at least three α-helices separated by loops and mediates head-to-tail assembly into heterodimers, which in turn can form a higher level of oligomerization, as seen in the core histone octamer [10]. For histone-like proteins, the HFD typically mediates protein–protein and protein–DNA interactions [12].

$ORP1^{HFD}$ and $ORP2^{HFD}$ share high sequence identity with the B and C subunits (56.4% and 50%, respectively) of the CCAAT-binding specific nuclear factor Y (NF-Y) [9]. Homology modeling, based on the NF-YB/YC heterodimer structure, was previously used to generate a putative model of the ORP1/2 HFD complex [4]. Interestingly, the occurrence of HFDs in non-nuclear proteins is rare, and to date, there is only one published example of a HFD-containing protein that functions out of the nucleus, a Ras-specific nucleotide exchange factor called Son-of-Sevenless (Sos) [13].

Mutant *P. berghei* oocysts, lacking the HFD of either ORP, do not rupture, underlining the functional relevance of the ORP dimer and suggesting the ORP1/2 interface as a promising druggable target for novel antimalarial therapies [4]. This potential is further enhanced by the differential intracellular locations of the interacting ORPs, offering a window of opportunity to administer inhibitory molecules that bind to the dimerization interface of either ORP, before they have a chance to meet. Targeting the mosquito stage of infection, rather than the human stage, also remains a relatively untapped strategy [14,15], primarily due to limited understanding of drug uptake mechanisms in

mosquitos and the absence of a well-established delivery platform. A possible means for administering ORP blockers includes using attractive targeted sugar bait (ATSB) strategies that lure mosquitos to a sugar suspension bait laced with the inhibitory molecule(s), or the use of organic or inorganic nanoparticles [14,16,17]. For an overview of nanodrug delivery systems in Malaria, see Kekani *et al.* [17]. However, a practical challenge encountered in testing such potential inhibitors lies in the inability to produce recombinant ORP HFDs in monomeric form. This limitation prevents the use of standard *in vitro* biochemical assays to assess binding affinities or to measure the inhibitors' capacity to block dimerization.

In this context, we present the first experimentally determined structure and in-depth structural analysis of the ORP1/2^{HFD} heterodimer, solved via X-ray crystallography at 3.1 Å resolution. We also describe the use of a yeast two-hybrid (Y2H)-based combinatorial library of cyclic peptides (CPs), named CYCLIC, to screen for candidates that prevent dimerization of ORP1^{HFD} with ORP2^{HFD}. From this screen, we successfully identified six CPs as potential dimerization inhibitors. *In silico* docking studies, using the ORP1^{HFD} monomer structure derived from our crystallographic data, revealed that identified CPs overlap with the region of several key interface residues of ORP2^{HFD}. We propose these CPs as potential dimerization inhibitors for further *in vivo* evaluation. Given the high conservation of the HFD interface across different species, ORP targeting peptides may have broader applications in diverse biological contexts.

Results

Heterologous production of the ORP1/2^{HFD} heterodimer

Multiple sequence alignments were carried out for the HFD regions of ORP1 (residues 774–839; Fig. 1A) and ORP2 (residues 23–109; Fig. 1B) across *Plasmodium* species, highlighting the strong conservation of this domain. Both domains displayed several invariant and highly conserved residues (Fig. 1A,B). Instead, Alphafold2-based 3D structure predictions for both individual full-length proteins and the ORP1/2 heterodimer [19] highlight the predominantly intrinsically disordered nature of both proteins outside the HFDs (Fig. 2A,B), as expected given the high frequency of asparagine-rich regions in their primary structures: 22.7% in ORP1 and 27.4% in ORP2. From an evolutionary perspective, amino acid expansions are typically not favored; however, *Plasmodium* is a well-known, intriguing exception to this rule, and asparagine repeats are commonly found in many *Plasmodium* proteins [22].

Considering that the only structured regions in both proteins largely pertain to the HFD that is necessary and sufficient for heterodimer formation [4], HFD constructs of both ORP1 and ORP2 were designed. The cDNAs for each ORP were cloned into two different plasmids and co-expressed in BL21(DE3) Star *Escherichia coli* cells, as described in the Methods section.

The ORP1/2^{HFD} heterodimer was purified via affinity chromatography, taking advantage of the N-terminal histidine tag fused onto ORP1^{HFD}, followed by size exclusion chromatography (SEC). The purified heterodimer eluted with an elution volume (V_e) of 20.9 mL, corresponding to a molecular weight (MW) of approximately 26 kDa, in line with the calculated MW of the heterodimer (26.3 kDa, including the His-tag) (Fig. 2C). Since ORP1^{HFD} and ORP2^{HFD} have calculated MWs of 13.2 kDa and 13.1 kDa, respectively, their bands were indistinguishable in SDS/PAGE analyses; therefore, western blotting of peak SEC fractions, using protein-specific antibodies, was carried out to confirm the presence of both proteins (data not shown).

3D structure of the ORP1/2^{HFD} heterodimer

The ORP1/2^{HFD} heterodimer crystallized in an orthorhombic space group $P2_12_12_1$, with six heterodimers (12 chains) in the asymmetric unit and a calculated Matthew's coefficient of 1.93 A^3/Da, corresponding to a solvent content of 36.4%. The ORP1/2^{HFD} structure was solved at 3.1 Å resolution by molecular replacement, as described in the Methods section, and refined to final R_{work} and R_{free} values of 0.274 and 0.295, respectively (Table 1: Fig. 2D). The refined structure presents good stereochemical parameters, with no Ramachandran outliers (Table 1).

Chains A, C, E, G, I, and K correspond to the ORP1^{HFD} monomer, whereas chains B, D, F, H, J, and L represent ORP2^{HFD}. Overall, electron density was better defined for ORP1^{HFD} than for ORP2^{HFD} and covered 774–860 residues in the best cases (chains C and E), and 774–855 in the worst resolved chain (K). In all ORP1^{HFD} chains, electron density was absent for the first 27 N-terminal residues (20 corresponding to the vector region and 7 to the ORP1^{HFD} sequence), indicating flexibility in this region. At the C terminus, density was missing for only one or two residues, except in chain K, which lacked five residues. With regard to ORP2^{HFD}, only chain D lacked

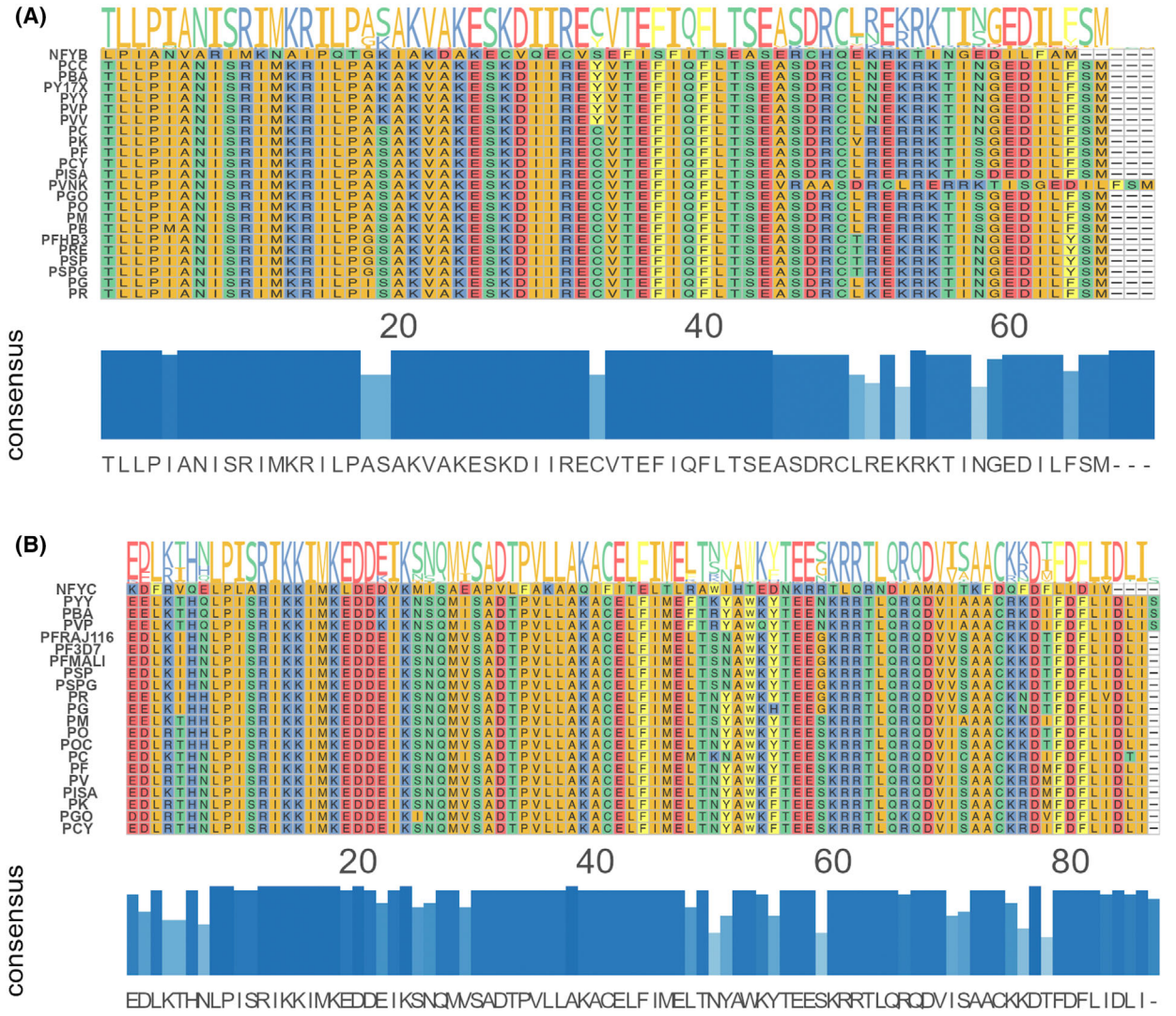

Color

Fig. 1. Multiple sequence alignment of the histone-fold domains of ORP1 and ORP2. The conserved histone-fold domain (HFD) regions of *Plasmodium berghei*: (A) ORP1^{HFD} (XP_034421376, residues 774–839, top) and (B) ORP2^{HFD} (XP_034423187, residues 23–109, bottom) were aligned with different *Plasmodium* species sequences. Human NF-YB and NF-YC histone-fold domains are also included as reference HFD sequences. Alignments were generated using MEGA12 and visualized with the ggmsa library in Rstudio [18]. Consensus residues are shown in single letter code, colored according to their charge and polarity, as follows: positive (blue), negative (red), polar uncharged (green), hydrophobic aliphatic (orange), and hydrophobic aromatic (yellow). Letter size indicates the level of conservation, with poorly and highly conserved residues in small and large letters, respectively. PCC, *Plasmodium chabaudi chabaudi*; PBA, *Plasmodium berghei ANKA*; PY17X, *Plasmodium yoelii 17X*; PYY, *Plasmodium yoelii yoelii*; PVP, *Plasmodium vinckei petteri*; PVV, *Plasmodium vinckei vinckei*; PC, *Plasmodium coatneyi*; PK, *Plasmodium knowlesi strain H*; PF, *Plasmodium fragile*; PCY, *Plasmodium cynomolgi strain B*; PISA, *Plasmodium inui San Antonio 1*; PVNK, *Plasmodium vivax North Korean*; PGO, *Plasmodium gonderi*; PO, *Plasmodium ovale*; PM, *Plasmodium malariae*; PB, *Plasmodium brasilianum*; PFHB3, *Plasmodium falciparum HB3*; PRE, *Plasmodium reichenowi*; PSP, *Plasmodium sp. DRC-Itaito*; PSPG, *Plasmodium sp. gorilla clade G3*; PG, *Plasmodium gallinaceum*; PR, *Plasmodium relictum*; PFRAJ116, *Plasmodium falciparum RAJ116*; PF3D7, *Plasmodium falciparum 3D7*; PFMALI, *Plasmodium falciparum MaliPS096 E11*; POC, *Plasmodium ovale curtisi*; PV, *Plasmodium vivax*; NF-YB, *Homo sapiens* NF-YB; NF-YC, *Homo sapiens* NF-YC.

internal gaps, whereas all other chains contained a gap around residues 42–48, corresponding to a flexible loop. Notably, chain L exhibited particularly higher flexibility at the N terminus and lacked density for the first 28 residues, in comparison with two to five missing residues in the other chains. As expected at this resolution, electron density was absent in some cases for particularly long, solvent-exposed sidechains (*e.g.*

Arg, Lys, and Glu). All structural analyses were carried out on the ORP1/2^{HFD} heterodimer comprising chains C and D that was the best-defined dimer in the electron density.

Based on structural annotations made with the PDBsum server (https://www.ebi.ac.uk/thornton-srv/databases/pdbsum/ [23]), both ORP proteins possess the canonical HFD (three α-helices and two connecting loops) with some variations (Fig. 2E,F). The ORP1^{HFD} monomer is built by four α-helices: three that comprise the HFD (α1-3) and one extra α-helix (αC), and two short β-strands (β1-2; Figs 2E, 3A). The ORP2^{HFD} monomer is comprised of five α-helices: three HFD helices (α1-3) and, as extra secondary structure elements, two α-helices (αN and αC), one 3^{10} helix (η1) and two β-strands (β1-2; Figs 2F, 3B). In the dimer, two parallel β-sheets are formed by β1 and β2 contributed by ORP1^{HFD} and ORP2^{HFD}, respectively and β2 and β1 by ORP1^{HFD} and ORP2^{HFD}, respectively (Fig. 2D).

The ORP1/2^{HFD} dimer adopts a compact structure, with a dimerization surface area of 2839.6 Å^2, and a binding free energy (ΔG) of −53.8 kcal/mol, as calculated by the PDBePISA server (Proteins, Interfaces, Structures and Assemblies; https://www.ebi.ac.uk/msd-srv/prot_int/) [27]. Each ORP^{HFD} subunit possesses a horseshoe-shaped cavity, lined by mainly hydrophobic amino acids that represent the principal interface residues (Fig. 4). Pocket analyses made with the CASTp-Fold server (https://cfold.bme.uic.edu/castpfold/ [28]) show that the ORP2^{HFD} cavity is narrower with respect to ORP1^{HFD}, with cavity volumes of 227.5 Å^3 and 1025.4 Å^3, respectively (Fig. 4A,B). The ORP1^{HFD} cavity (Fig. 4A) is lined by 17 nonpolar and only 2 polar/charged amino acids (R787 and D846), whereas the ORP2^{HFD} cavity (Fig. 4B) is lined by 9 nonpolar and 2 polar/charged (E41 and D42) amino acids. In both ORP monomers, α2 forms the base of the cavity, and α1 forms one side. The opposite side instead is formed by α3 in ORP1^{HFD} and η1 and αC in ORP2^{HFD} (Fig. 4).

Each subunit clasps together, forming a tightly packed heterodimer with extensive hydrophobic contacts and 23 hydrogen bonds (Table 2). Previous structural studies, analyzing plant NF-YB and NF-YC subunits, deduced that shape complementarity is more relevant than specific residue–residue interactions in heterodimerization [29].

In line with typical HFD-containing proteins, analysis of the surface electrostatics reveals the presence of a long basic patch that extends along one side of the dimer, formed by the clustering of arginine and lysine residues present in α1, the first few residues of α2 and the loop connecting these two secondary structure elements in ORP1^{HFD}, and α1 and the loop connecting α1 and α2 in ORP2^{HFD} (Fig. 5A). This basic region corresponds to the protein–DNA interface region in HFD-containing DNA-binding complexes and is highly conserved at a structural and sequence level (Fig. 3) [9,25,29]. As previously mentioned, the ORPs are not found in the nucleus; therefore, this basic patch is likely to have an alternative function that remains to be seen, for example, it may interact with the intrinsically disordered regions in the full-length proteins or it could mediate interactions with other protein partners. In the Alphafold-predicted full-length dimer structure, the basic stretch is solvent-exposed and may therefore be available to interact with other regions of the protein structure (Fig. 2A). However, due to the intrinsically disordered nature of the regions outside the HFD that are predicted with low confidence, it remains unclear whether and how such interactions might occur.

Unsurprisingly, due to the extensive positively charged surface regions, five sulfate ions, derived from the crystallization solution, were found bound in the asymmetric unit and appear to stabilize neighboring subunits. Three of these anions are bound to ORP1^{HFD} chains (A, C, and I), interacting with the main chain amide nitrogen between K828 and T829 that compose β2. The remaining three sulfate ions are bound to ORP2^{HFD} chains, each interacting with the nitrogen atom of the R84 sidechain (present in β2), thereby stabilizing adjacent ORP2^{HFD} monomer pairs (chain B and symmetry-related chain J; chains D and F, and chains H and L).

Protein structure comparisons were made using ORP chains C and D and the DALI server (http://ekhidna2.biocenter.helsinki.fi/dali/) [31]. The *Arabidopsis thaliana* NF-Y subunit B6 (*At*NFYB; PDB code 5G49) was identified as the top structural homolog of ORP1^{HFD}, with over 87 out of 97 aligned residues (54% sequence identity; RMSD 1.1 Å; Z-score 12.4) (Fig. 3) [17]. The highest structural homolog of ORP2^{HFD} instead is the HapC subunit of the CCAAT-binding complex from *Aspergillus nidulans* (*An*HapC; PDB: 6Y37; 11.6 Z-score, RMSD of 1.6 Å over 100/118 aligned residues with 46% sequence identity) [25,31] (Figs 3, 5B).

To better visualize the regions of sequence and structural diversity between the ORPs and their structural homologs, sequence and structure-based comparisons were made against proteins deposited in the PDB (with an *E*-value cutoff of 1×10^{-6}), using the ENDScript 2.0 server (https://endscript.ibcp.fr/ESPript/ENDscript/) [30](Fig. 5C,D). Overall, the HFD fold is

well conserved both in sequence and structure, with only some loops and the termini of the proteins that exhibit some structural variation (Fig. 5C). Nonconserved residues in ORP1^{HFD} are distributed throughout the structure and do not cluster in a specific region, thus preserving the overall HFD architecture (Fig. 5C).

For ORP2^{HFD}, a complete lack of sequence conservation was observed in N-terminal residues 5 to 23 that form αN and a loop region that connects this helix to α1 (Fig. 5D). Other nonconserved residues are scattered throughout the structure and do not localize to a particular region.

In vitro dimerization of ORP1^{HFD} and ORP2^{HFD} assessed by yeast two-hybrid assay

To evaluate whether *Saccharomyces cerevisiae* could function as a suitable *in vitro* system to screen ORP-interacting molecules, we first tested the expression and dimerization of ORP^{HFD} proteins in this organism. The cDNAs encoding each ORP1^{HFD} and ORP2^{HFD} were cloned in-frame with the GAL4 DNA-binding domain (DBD) and activation domain (AD), respectively, as described in the Methods section. After excluding possible autoactivation of the ORP1^{HFD} bait protein, the Y2HGold yeast strain was co-transformed with ORP1^{HFD} and ORP2^{HFD} plasmids, resulting in successful colony growth. The reporter gene activation in the presence of both prey and bait proteins was indicative of heterodimer formation. Expression of the fusion proteins in yeast was further confirmed by western blotting, using antibodies specific for the DBD or AD (Fig. 6A). To assess the specificity of this interaction *in vivo*, an 'absence of interference test' was performed (see the Methods section). Briefly, a mutant library of ORP2^{HFD}, containing 2037 individual clones, was generated via error-prone PCR, and clones that demonstrated an interaction with ORP1^{HFD}, despite mutations, were retrieved using yeast mating. From a screening of $2.4*10^6$ mL^{-1} diploids on selective media, we obtained 680 CFU·mL^{-1}. After further selection on more stringent media, 44 clones were sequenced, retrieving 39 unique sequences. Overall, these variants showed 7.5% of total mutations (1.5% synonymous and 6% nonsynonymous). Of the 111 residues that comprise the ORP2^{HFD} construct, 38 residues (34%) remained unvaried among clones. Notably, the most highly conserved residues were concentrated at the ORP1/2^{HFD} interaction interface (Fig. 6B).

Identification of cyclic peptides as potential dimerization blockers

Given the essential requirement of ORP1/2^{HFD} dimerization for oocyst rupture, sporozoite egress and ultimately *Plasmodium* infection progression, we targeted the dimerization interface of ORP1^{HFD} for inhibitor discovery. Targeting a protein interface raises the possibility of designing peptides that mimic the protein–protein interaction interface. However, a major limitation in rational design of peptides, based on the ORP1/2^{HFD} crystal structure, is the inability to heterologously express ORP1^{HFD} alone for *in vitro* binding assays. To overcome this issue, we employed a Y2H-based approach to screen CYCLIC, a combinatorial library of CPs to identify ORP1^{HFD} binders [32]. Initial Y2H screening retrieved 90 colonies, grown on selective media that were sampled for yeast colony PCR and sequencing to identify ORP1^{HFD}-CPs. The ORP1^{HFD}-CP sequence list underwent a round of refinement in which the new CP list was compared with a list of CPs known to be GAL4-DBD interactors. This filtering process refined the ORP1^{HFD}-CP list to 41 CP sequences that were experimentally assayed for their ability to interact with ORP1^{HFD} or the GAL4-DBD scaffold of the Y2H assay. Testing ORP1^{HFD}-CPs against the target proteins (either ORP1^{HFD} or GAL4-DBD) allowed six ORP1^{HFD}-CPs

Color

Fig. 2. The *P. berghei* ORP1/ORP2^{HFD} dimer. (A) The full-length oocyst rupture protein (ORP) heterodimer, predicted using Alphafold2 [20], with the histone-fold domain (HFD) of ORP1^{HFD} and ORP2^{HFD} chains in pale pink and pale blue ribbons, respectively. The crystal structure of the ORP1/2^{HFD} dimer is also shown, superposed with the full-length dimer, with ORP1^{HFD} and ORP2^{HFD} in magenta and blue ribbons, respectively. (B) Detailed view of the superposition of the ORP1/2 crystal structure with the Alphafold2 model, trimmed to the HFD region. The N- and C termini are labeled for both ORP HFDs, indicating which by numbers in brackets. The crystal structure was determined using X-ray diffraction data from a single crystal (Table 1). (C) Size exclusion chromatography (SEC) profile of the ORP1/2^{HFD} dimer (illustrative of a typical purification carried out at least three times), following the absorbance at 280 nm in milli-absorbance units (mAU) relative to volume (mL). The elution volume (V_e) of 20.6 mL for the ORP1/2^{HFD} dimer is shown. (D) Secondary structure representation of the ORP1/2^{HFD} dimer comprising chains C (ORP1^{HFD}) and D (ORP2^{HFD}) in magenta and blue ribbons, respectively. The N- and C termini are labeled, as are the secondary structure elements. (E) The ORP1^{HFD} fold shown in ribbons. (F) The ORP2^{HFD} fold shown in ribbons. In panels E and F, α-helices and β-strands, not present in the canonical HFD, are colored orange and yellow, respectively. All panels except for panel B were generated using ChimeraX version 1.8 [21].

5

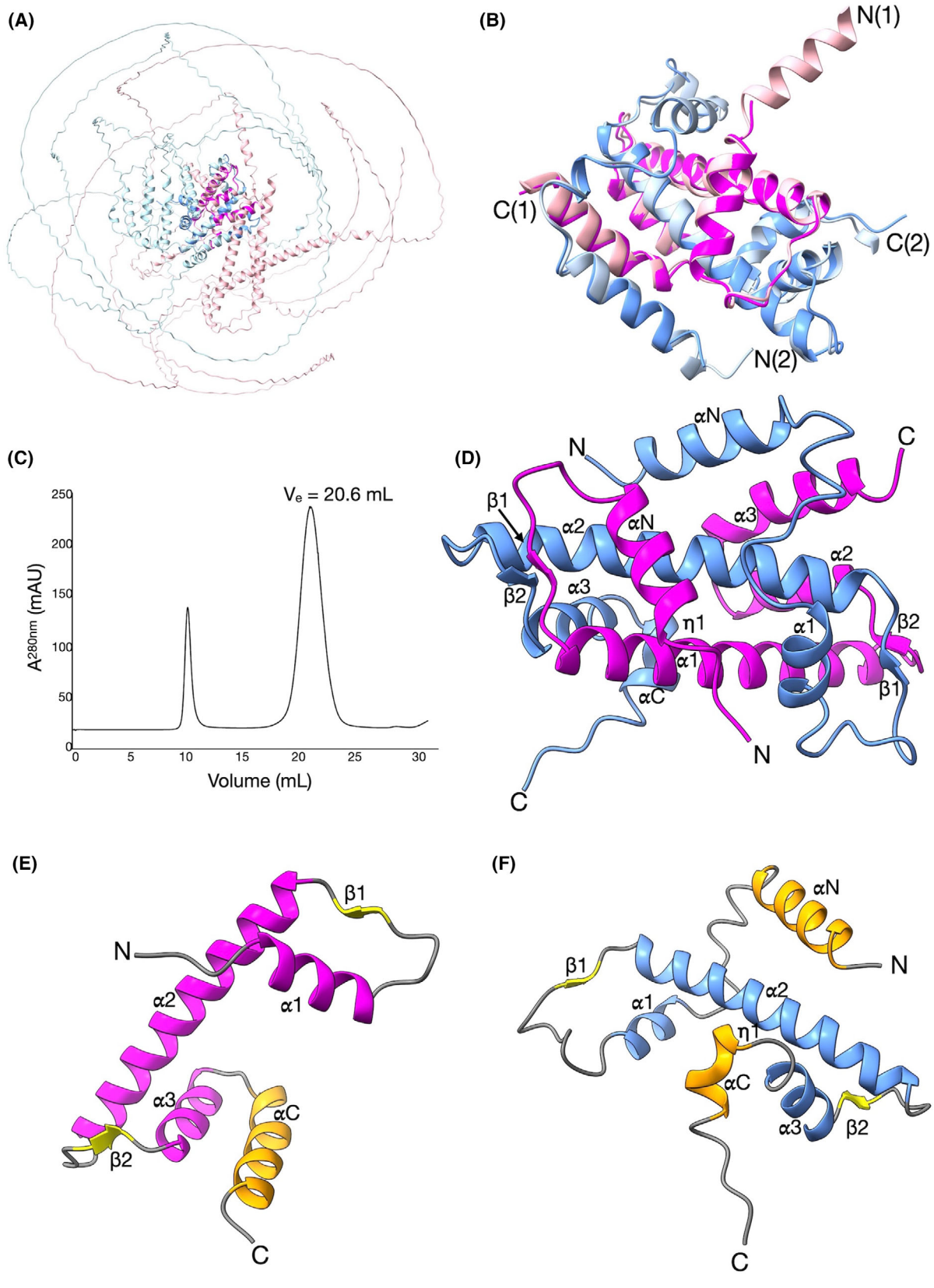

Table 1. X-ray data collection and refinement statistics for the ORP1/2^{HFD} crystal.

	ORP1/2^{HFD} (PDB code 9RIF)
Crystal	
Space group	$P2_12_12_1$
Unit cell dimensions	82.7, 112.9, 145.2
a, *b*, *c* (Å); α, β, γ (°)	90.0, 90.0, 90.0
Data collection	
Beamline	ESRF ID23-2
Wavelength (Å)	0.873
Resolution (Å)	82.7–3.1 (3.3–3.1)
Total reflections	335 066 (62581)
Unique reflections	25 331 (4518)
R_{merge} [b]	0.175 (1.295)
R_{meas} [c]	0.189 (1.395)
$I/\sigma(I)$	12.0 (2.3)
$CC_{1/2}$ [d]	0.997 (0.849)
Completeness (%)	99.8 (99.8)
Average redundancy	13.2 (13.9)
Wilson B-factor (Å)	77.3
Refinement	
Resolution (Å)	66.7–3.1
No. reflections	25 265 (2471)
R_{work}/R_{free}	0.274/0.295
No. atoms in asymmetric unit	
Protein	9069
Water	18
Sulfate ions	30
Ethylene glycol	4
B factors (Å^2)	
Protein	77.2
Water	57.8
Sulfate ions	103.7
Ethylene glycol	68.4
RMSD	
Bond lengths (Å)	0.006
Bond angles (°)	0.841
Clashscore	5.92
Ramachandran	
Favored (%)	96.6
Allowed (%)	100

[a]Values in parenthesis correspond to the high-resolution shell. For cross-validation, 5% experimental reflections were randomly selected to calculate the R_{free} value; [b]$R_{merge} = \Sigma_h \Sigma_i |<I_h> - I_{h,i}| / \Sigma_h \Sigma_i I_{h,i}$; [c]$R_{meas} = \Sigma_h [N_h/(N_h - 1)]^{1/2} \Sigma_i |<I_h> - I_{h,i}| / \Sigma_h \Sigma_i I_{h,i}$, where N_h is the data multiplicity; [d]$CC_{1/2}$ is the correlation coefficient of the mean intensities between two random half-sets of data.

to be identified, representing promising candidates for further development as dimerization inhibitors (Fig. 6C).

In silico docking of cyclic peptides to ORP1^{HFD}

Since ORP1^{HFD} cannot be produced as an isolated subunit, direct *in vitro* evaluation of CP binding to ORP1^{HFD} is not feasible. However, taking advantage of the available ORP1/2^{HFD} crystal structure, *in silico* docking was carried out with the Schrödinger Maestro suite to estimate the binding mode of the six ORP1^{HFD}- CPs, ranking them in order of priority for *in vivo* testing, based on their calculated docking scores (see the Methods section). The most promising docking poses were selected by prioritizing models whose peptide interaction patterns and residue contacts closely resembled those of ORP2^{HFD} at its dimerization interface with ORP1^{HFD} (Fig. 7). The six CPs can be divided into two groups: three (CP3, CP8, and CP35) that dock at the ORP1^{HFD} cavity and align with ORP2^{HFD} residues that are contributed by α3 and αC (**C site**), and three (CP36, CP71, and CP78) that dock at the other side of the cavity with residues contributed by ORP2^{HFD} α1 (**N site**) (Fig. 7; Table 3).

Among the six peptides, the pose selected for CP3 (sequence: IMSSLRWW; docking score: −6.016) most closely mimics the interactions of ORP2^{HFD} with ORP1^{HFD} (Fig. 8A). Specifically, CP3 I1 coincides with a hydrophobic core region (**C site**) of ORP2^{HFD} defined by F66, I100, F101, and L104 from αC, and protrudes toward F810 and F844 of ORP1^{HFD}, located in α2 and the loop between α3 and αC helices, respectively. The counterpart of CP3 M2 is represented by V91 and A95 in ORP2^{HFD}. CP3 S3 resembles ORP2^{HFD} T71, while CP3 S4 is solvent-exposed in the model. CP3 L5 extends toward ORP1^{HFD} I788, analogous to ORP2^{HFD} F9. CP3 R6 mirrors the position of ORP2^{HFD} residues R97 and K98, and in the docking model forms both a salt bridge and a hydrogen bond with ORP1^{HFD} D846, interactions not observed in the crystal structure. CP3 residues W7 and W8 align with ORP2^{HFD} I67 and M68, establishing a hydrophobic core that interfaces with the ORP1^{HFD} α-helices 1 and 2, specifically contacting residues I781, I784, I788, I803, and V807 (Fig. 8A; Table 3).

The selected pose for CP8 (sequence: IWYGGGWW; docking score: −3.397) was the only model obtained without Prime macrocycle sampling (Fig. 8B; see Methods). In this configuration, CP8 residue I1 mostly overlaps the region occupied by ORP2^{HFD} residues V91 and I92 present in α3. CP8 residue W2 protrudes toward α2 of ORP1^{HFD}, overlaying ORP2^{HFD} residues F101, F103, L104, and L107 in αC. CP8 residue Y3 is located near ORP2^{HFD} Y73. CP8 residue W7 is superimposable with ORP2^{HFD} I67 and is near L30, becoming buried within the ORP1^{HFD} hydrophobic core at the interface between helices α1 and α2. Finally, CP8 residue W8 resembles ORP2^{HFD} W75, establishing hydrophobic interactions in the vicinity of ORP1^{HFD} L789 (Fig. 8B).

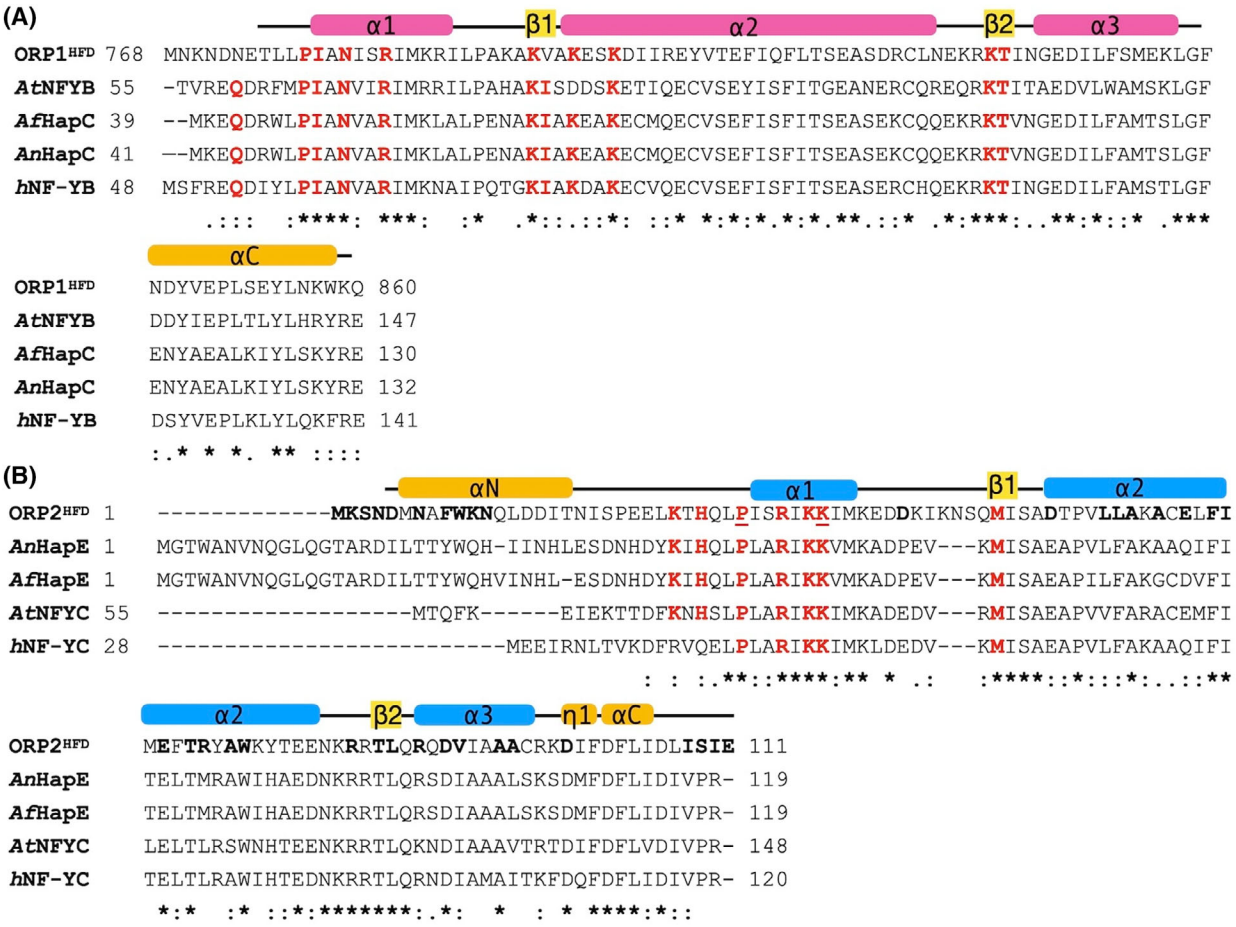

Color 7

Fig. 3. Sequence conservation of the ORP1/2^{HFD} dimer. (A) The amino acid sequences corresponding to residues 768–860 of the histone-fold domain (HFD) of ORP1 and top structure homolog: *A. thaliana* NF-YB (*At*NFYB; PDB:5G49; [24]), *A. fumigatus* HapC (*Af*HapC; PDB: 6Y36; [25]), *A. nidulans* HapC (*An*HapC; PDB:6Y37; [25]) and human NF-YB (*h*NF-YB; PDB:4AWL; [9]), were aligned using the Clustal Omega server [24,26]. (B) Amino acid residues 1–111 of ORP2^{HFD} were aligned with *A. nidulans* CBDF (*An*HapE; PDB:6Y37 [25]), *A. fumigatus* HapE (*Af*HapE; PDB: 6Y36; [25]), *A. thaliana* NF-YC (*At*NFYC; PDB:5G49 [24]) and human NF-YC (*h*NF-YC; PDB:4AWL [9]). Identical residues, conservative and semi-conservative substitutions are indicated by an asterisk, colon and full stop, respectively. Conserved DNA-binding residues that interact with DNA (via main chain or side chain atoms) with interaction distances (<3.8 Å), identified in the DNA-bound CCAAT-binding complex (PDB: 6Y36) and top structure homolog, are highlighted in red bold font. Residues in black, bold font indicate the 38 invariant residues observed in error-prone polymerase chain reaction yeast two-hybrid studies. Two of these residues (P31 and K37) are also conserved DNA-binding residues and are underlined to distinguish them. Secondary structure elements for ORP1^{HFD} and ORP2^{HFD} are shown above, with secondary structure coloring as in Fig. 2.

The CP35 (sequence: CRRIASIY) pose yielded the highest docking score (−6.413). In this model, CP35 residue C1 corresponds to the region of ORP2^{HFD} encompassing F66, F103, and L104, in proximity to C96. CP35 R2 aligns with ORP2^{HFD} R88 and can establish a hydrogen bond with ORP1^{HFD} Y806. CP35 R3 mirrors ORP2^{HFD} R97 and K98 and forms salt bridges with ORP1^{HFD} D846 on αC and a hydrogen bond with the backbone of G843. CP35 residues I4, A5, and I7 mimic the ORP2^{HFD} hydrophobic core constituted by F70, I92, A93, V91, and A94. CP35 S6 aligns with ORP2^{HFD} T71, while CP35 Y8, although lacking a direct ORP2^{HFD} counterpart, is situated close to the hydrophobic residues of ORP1^{HFD} on the α2 helix (residues V807, F810, I811) (Fig. 8C).

The pose for CP36 (sequence: ALSQFIIK; docking score: −4.808) differs in location from the previously described poses and docks to the N site, toward helix α1 of ORP2^{HFD}. CP36 residues A1 and L2 align with ORP2^{HFD} A60 and L59, respectively. CP36 S3 and Q4 do not have direct counterparts in ORP2^{HFD}; however, Q4 can establish a hydrogen bond with the

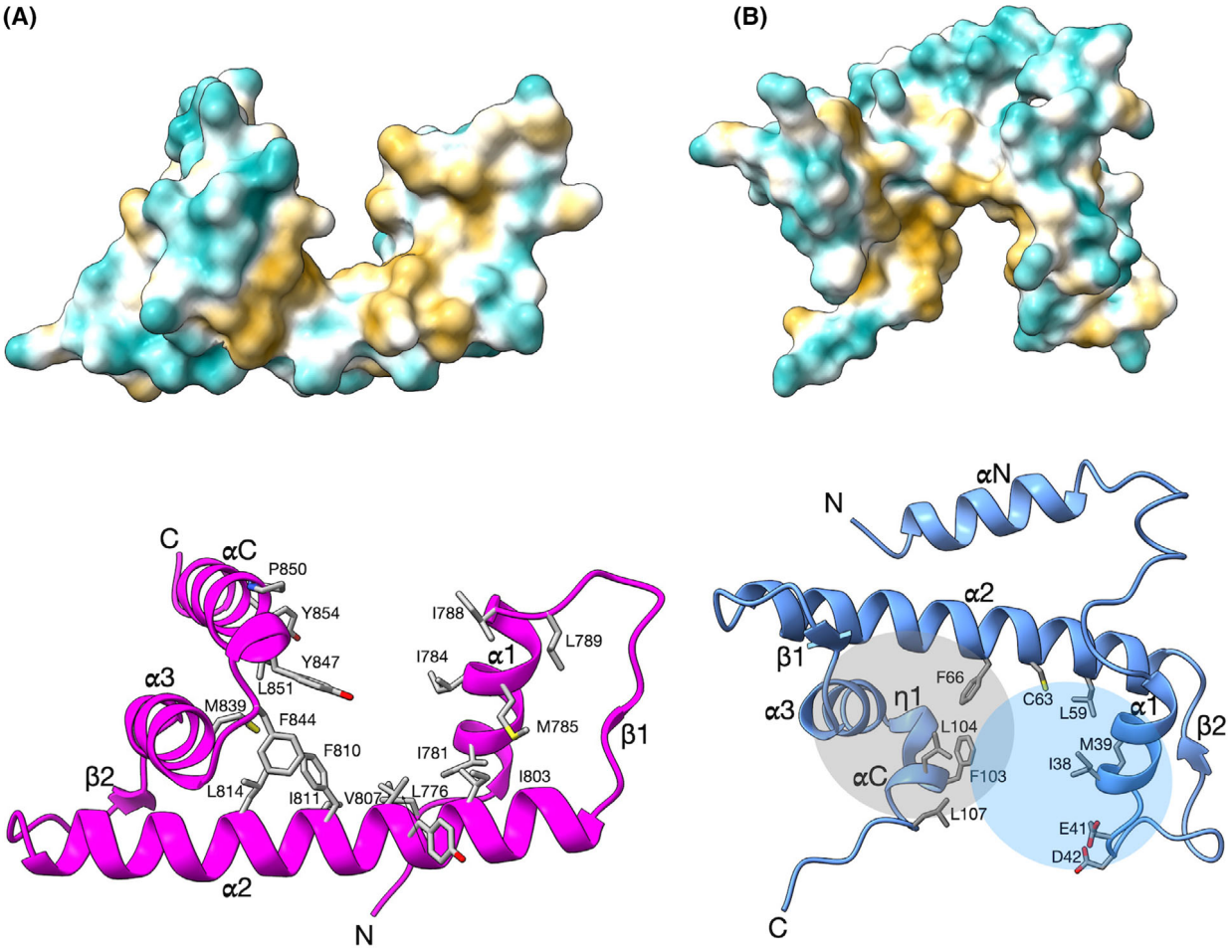

Color

Fig. 4. Hydrophobic interfaces in the oocyst rupture protein histone-fold domains. Surface representation of the histone-fold domain (HFD) of ORP1 (A) and ORP2 monomers (B), with surface coloring according to residue hydrophobicity, with yellow coloring indicating maximum hydrophobicity to white and turquoise, representing the maximum hydrophilicity. The surface representations in the upper panels reflect the orientations of the corresponding ribbon representations in the lower panels. The lower panels show the residues that line the cavities, as calculated using CASTpFOLD [28], in stick format, colored according to heteroatom and labeled. The N site and C site of ORP2^{HFD} are indicated by shaded circles in gray and blue, respectively. The N- and C termini are labeled, as are the secondary structure elements. This figure was generated using ChimeraX version 1.8 [21].

backbone of ORP1^{HFD} G832. CP36 F5 aligns with ORP2^{HFD} L65 and is oriented toward ORP1^{HFD} L851, while CP35 I6 and I7 overlap with the region occupied by ORP2^{HFD} I32 and V57. CP36 K8 aligns with the position of ORP2^{HFD} K36, K40, and K44, and in the model, forms a hydrogen bond with the backbone of ORP1^{HFD} I830 (Fig. 9A).

CP71 (sequence: MMFAILNV; docking score: −4.370) shares a similar binding region to CP36 toward site N. In its docking pose, CP71 M1 and M2 align with ORP2^{HFD} M39 and V57, respectively, while CP71 F3 extends into the region occupied by the side chains of ORP2^{HFD} L58 and L65 (Fig. 9B). CP71 A4 superimposes with ORP2^{HFD} A53, and CP71 I5 aligns with ORP2^{HFD} I51, as does CP71 L6. Although there is no closer counterpart for CP71 N7, it can establish a hydrogen bond with ORP1^{HFD} T815. CP71 V8 aligns with ORP2^{HFD} I35 and I38 and is embedded within the hydrophobic region of ORP1^{HFD} defined by L776 at the N terminus and I811 on the α2 helix (Fig. 9B).

CP78 (sequence: RRTYSVLL; docking score: −4.523) also binds within the same ORP1^{HFD} region as CP36 and CP71. CP78 R1 aligns to ORP2^{HFD} R34 and extends toward ORP1^{HFD} T774, while CP78 R2 mimics ORP2^{HFD} K40 and K44 and establishes hydrogen bond interactions with ORP1^{HFD} T815 (Fig. 9C). CP78 T3 is solvent-exposed and resembles ORP2^{HFD}

Table 2. Summary of the hydrogen bonds formed at the ORP1/2^{HFD} dimer interface.

ORP1^{HFD} residues	ORP2^{HFD} residues	Bond length (Å)
THR774(OG1)	ARG34(NH2)	3.61
LEU775(O)	ARG34(NE)	2.75
ILE788(O)	ARG72(NH1)	2.56
LYS794(O)	LEU86(N)	2.76
GLU798(OE2)	ARG88(N)	3.40
SER799(OG)	ARG88(N)	3.78
LYS828(O)	MET50(N)	3.33
ILE830(O)	SER52(N)	2.94
ILE830(O)	THR55(OG1)	3.74
THR774(N)	GLU41(OE2)	3.77
ASN780(ND2)	GLN29(O)	2.50
ARG787(NH2)	GLN29(OE1)	3.15
LYS794(N)	ARG84(O)	2.87
ALA796(N)	LEU86(O)	3.17
SER799(OG)	LEU86(O)	2.72
SER819(OG)	ASP 43(O)	3.59
SER819(OG)	GLN49(OE1)	2.82
CYS822(SG)	GLN49(OE1)	3.37
LYS828(NZ)	SER48(O)	2.54
ILE830(N)	MET50(O)	3.05
GLY832(N)	ASP54(OD1)	3.32
TYR847(OH)	GLU69(OE1)	2.28
LYS857(NZ)	THR18(O)	2.45

The atoms involved in the hydrogen bond are shown in parenthesis, together with the bond lengths in Å. Interface residues were identified using chains C (ORP1^{HFD}) and D (ORP2^{HFD}) and the PDBePISA server [27].

T27. Although CP78 Y4 and S5 lack direct counterparts on ORP2^{HFD}, they form hydrogen bonds with ORP1^{HFD} N831 and the backbone of L851. CP78 V6 aligns with ORP2^{HFD} L59 and inserts into the hydrophobic interface between the α1 and α2 helices of ORP1^{HFD}, defined by residues F810, L814, and I835. CP78 L7 and L8 overlay the region occupied by ORP2^{HFD} L30, I35, and A60 (Fig. 9C).

In summary, all six CPs dock at the ORP1^{HFD} dimerization interface and adjacent regions, with binding localized primarily to either the ORP2^{HFD} α3 and αC helices (as seen with CP3, CP8, and CP35) or the α1 helix (as observed for CP36, CP71, and CP78). The hydrophobic interface residues are highly conserved between ORP1^{HFD} and NF-YB, suggesting that identified CPs may also have uses for other HFD-containing proteins in different biological contexts. (Fig. 10).

Discussion

HFDs are protein modules typically found in histones and certain transcription factors, such as CCAAT-binding proteins. However, given the non-nuclear localization of ORP proteins, a DNA-binding function for their HFDs is unlikely. Instead, the ORP1/2^{HFD} crystal structure underscores the critical role of these regions in mediating heterodimerization, similarly to the Sos protein, the only other known example of an HFD-containing protein functioning outside the nucleus [13]. Sos is a multi-domain, Ras and Rac guanine nucleotide exchange factor that is activated by growth factor receptors, which induce its relocation from the cytoplasm to the membrane, where it binds to a small G protein Ras, triggering GDP to GTP exchange [13,33]. Notably, this intracellular relocation parallels the behavior of ORP2 which moves from inside the oocyst to the outer capsule, immediately before oocyst rupture [4].

Protein complex formation is central to many biological processes and in *Plasmodium*, dimerization of ORP1 and ORP2, via their HFDs, is essential for oocyst rupture and infection progression [3,4]. Thus, preventing this protein–protein interaction represents a promising and novel strategy to block oocyst rupture and consequently, parasite transmission.

We analyzed the molecular details of the HFD-mediated ORP heterodimerization and we identified six CPs that interact with ORP1^{HFD} using a Y2H assay. ORP1^{HFD} was selected as the target for inhibitor discovery due to its stable localization in the cyst capsule, which offers a consistent and accessible therapeutic window, unlike ORP2^{HFD}, whose localization shifts from the cyst interior to the capsule only immediately before oocyst rupture. This changing localization of ORP2^{HFD} also makes it a less practical target with respect to ORP1^{HFD}. Since it is not possible to carry out *in vitro* binding studies between identified CPs and recombinant ORP1^{HFD}, due to the inability to produce HFDs in isolated monomeric form, *in silico* molecular docking analyses were carried out, revealing that all six identified CPs target the ORP1^{HFD} dimerization interface, mimicking the binding mode of ORP2^{HFD} found in the ORP1/2^{HFD} crystal structure. Collectively, the docking models indicate that the CPs span a broad surface area of the ORP1^{HFD} interface, particularly targeting the inner hydrophobic core of the ORP1/2^{HFD} interface, corresponding to the position of helix α2 in ORP2^{HFD} (Fig. 4B). The ability of the CPs to consistently bind in this hydrophobic groove, recapitulating the native ORP1/2^{HFD} interactions, underscores its potential as a critical anchor point for inhibition. Additionally, the peptides also extend into adjacent interface regions, predominantly covering either the ORP2^{HFD} αC helix (CP3, CP8, and CP35) or the α1 helix (CP36, CP71, and CP78), further mirroring the native heterodimer interaction surface (Fig. 2). In terms of docking performance, CP35 and CP3 achieved the best scores, while the remaining four

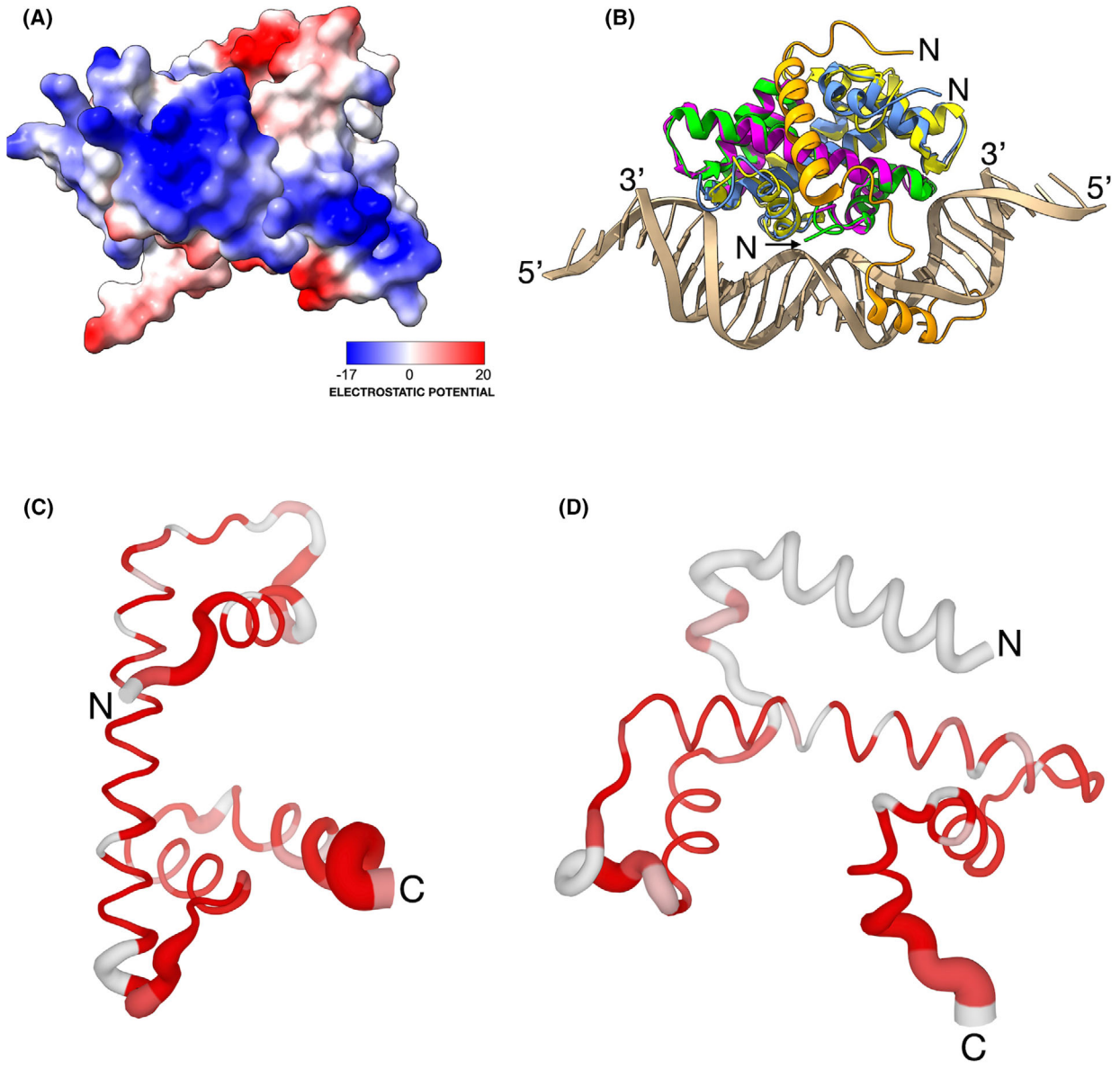

Color

Fig. 5. Comparison of the ORP1/2^{HFD} dimer with the *A. nidulans* CCAAT-box binding complex. (A) Surface representation of the ORP1/2 histone-fold domain (HFD) dimer in the orientation shown in Fig. 2D, colored according to electrostatic potential, illustrating positive (blue) and negative (red) regions. The electrostatic potential scale bar (units in kcal/(mol*e)) is shown. (B) Superposition of the ORP1^{HFD} (magenta) and ORP2^{HFD} (light blue) dimer with the crystal structure of *A. nidulans* CCAAT-box binding complex (PDB code 6Y37; [25]), comprising subunits HapB (orange ribbons), the HFD-containing HapC (green ribbons), and HapE (yellow ribbons), bound to DNA (beige ribbons) [25]. The N termini of each subunit of the *A. nidulans* trimer are shown, as are the 5′ and 3′ extremities of the DNA helix. (C) Sequence and structure conservation of ORP1^{HFD} with structure homologs in the protein data bank (PDB). (D) Sequence and structure conservation of ORP2^{HFD} with structure homologs in the PDB. In panels C and D, sequence and structure comparisons of the PDB were made using ENDScript 2.0 [30] and backbone atoms are represented as tubes and colored according to sequence conservation (gray to dark red, indicating low to high sequence conservation). Tube radius is proportional to the differences in Cα position between the ORP input structure and identified structural homologs (sequence identity cutoff 50%). Panels A and B were prepared using ChimeraX 1.8 [21], whereas panels C and D were generated using PyMol (http://www.pymol.org/pymol).

CPs showed similar but lower docking scores, suggesting that *in vivo* testing should prioritize the two top ranking peptides.

Compared with linear peptides, CPs offer significant advantages, including higher binding affinities, specificity, and resistance to proteolysis, since they lack the

terminal amine and carboxylic acid groups that are accessible to exopeptidases [34]. In addition, access to the cleavage site of endopeptidases is hindered. Their cyclic structure also limits conformational flexibility, increases surface area for target interaction, and improves cell membrane permeability since their rigid structure lowers the energy barrier required for the peptide to adapt to the membrane environment and bind to transport proteins to enter the cell by passive diffusion or active transport [32,34]. Altogether, these features make them amenable to develop new drugs, as witnessed by the over 50 CP-based therapeutics approved by different regulatory authorities [35].

Targeting the mosquito phase, and particularly the oocyst, for Malarial drug development offers an interesting alternative to targeting the human phase of infection, although it must be noted that research on this phase is lacking and the exact capsule composition remains to be seen. Therefore, a significant amount of preliminary knowledge on the mechanism of drug uptake in the mosquito, together with drug delivery optimization, must be undertaken prior to *in vivo* tests. Once such information is available, we propose the six CPs identified in our study as candidates for *in vivo* testing in mosquitos to evaluate their future potential to block oocyst rupture.

Methods

Sequence alignments of ORP1^{HFD} and ORP2^{HFD}

A BLAST search was performed using the HFD of the *Plasmodium berghei* ORP1 (XP_034421376, residues 774–839) and ORP2 (XP_034423187, residues 23–109) as queries. Similar sequences from different *Plasmodium* species were retrieved and subsequently aligned. Multiple sequence alignments were generated using MEGA 12 [18], and the resulting outputs were imported into R Studio for further processing. The alignments were visualized and exported with the *ggmsa* library.

Cloning of ORP1^{HFD} and ORP2^{HFD} for yeast two-hybrid assay

ORP1^{HFD} and ORP2^{HFD} cDNA were amplified by PCR using Phusion High Fidelity DNA polymerase (New England Biolabs) and buffer HF, using specific primers and the following protocol: 5 min denaturation at 95 °C, 15 cycles of denaturation at 95 °C for 10 s, annealing at 55 °C for 30 s, and elongation at 72 °C for 30 s, followed by 25 cycles of denaturation at 95 °C for 10 s, and annealing/elongation at 72 °C for 30 s and a final elongation step of 5 min at 72 °C.

Amplified PCR products were cloned into pGBKT7 and pGADT7 vectors, respectively, via *EcoRI* and *BamHI* restriction enzyme sites using the In-Fusion HD Cloning Plus kit (Takara Bio USA) and sequenced (Eurofins Genomics, Ebersberg, Germany). Recombinant plasmids were transformed into *E. coli* Stellar Competent Cells. Vectors, enzymes, and Stellar cells were purchased from Clontech.

Co-transformation and testing bait for autoactivation

The *S. cerevisiae* Y2HGold strain (Clontech, USA) was transformed with the above-mentioned constructs, according to the manufacturer's instructions (Yeastmaker Yeast Transformation System 2 User Manual), following the small-scale transformation protocol. Y2HGold includes the Aureobasidin A (AuA)-sensitive antibiotic resistance gene (Clontech) as a reporter. Three additional reporter constructs, ADE2, HIS3, and MEL1 that are only expressed in the presence of GAL4-based protein interactions, were also included.

Yeast cells were transformed with 100 ng pGADT7, pGBKT7, pGADT7-ORP2^{HFD}, or pGBKT7-ORP1^{HFD} and plated on Single Dropout (SDO)/-Leucine (Leu) media for pGADT7 or SDO/-Tryptophan (Trp) for pGBKT7, in the presence or absence of AuA (200 ng·mL^{-1}) and X-α-gal (40 µg·mL^{-1}) (Clontech) to exclude autoactivation of the GAL4 promoter by the GAL4 BD-ORP1^{HFD} fusion protein.

The Y2HGold strain was co-transformed with 100 ng each of pGBKT7-ORP1^{HFD} and pGADT7-ORP2^{HFD} and plated on Double Dropout (DDO)/-Leu/-Trp media in the presence or absence of AuA (200 ng·mL^{-1}) and X-α-gal (40 µg·mL^{-1}) to confirm the interaction between the two HFDs. Transformants were further plated on Quadruple dropout (QDO) -Leu/-Trp/-Adenine (Ade)/-Histidine (His) media for additional selection. Transformations and co-transformations were performed following the manufacturer's protocol (Yeastmaker Yeast Transformation System 2 User Manual, Takara) and Yeast Protocols Handbook guidelines (Takara), respectively.

Random mutagenesis of ORP2^{HFD} and Y2H assay

A library of randomly mutated ORP2^{HFD}, expressed in Y2HGold-pGADT7 was screened for interaction with wild-type ORP1^{HFD}-pGBKT7, expressed in yeast strain Y187, via the Y2H assay. The assay was performed according to the Matchmaker Gold Yeast Two-Hybrid System User Manual guidelines.

Saccharomyces cerevisiae strain Y187 (Clontech, USA) was transformed with ORP1^{HFD}-pGBKT7, according to the manufacturer's instructions (Yeastmaker Yeast Transformation System 2 User Manual), following the small-scale transformation protocol.

Random mutagenesis of the ORP2^{HFD} transcript was performed by error-prone (ep) PCR. The epPCR reaction mixture (50 μL) contained 10 mM Tris–HCl pH 8.4, 50 mM KCl, 7 mM $MgCl_2$, 5 mM $MnCl_2$, biased nucleotide composition (1 mM each of dCTP and dTTP, 0.2 mM each of dATP and dGTP), 500 nM each of specific primers, 1% (*v*/*v*) dimethyl sulfoxide (DMSO), 1.6 U GoTaq DNA Polymerase (Promega), and 1.5 pg of DNA template. PCR products were analyzed on a 1.2% (*w*/*v*) agarose gel, purified, and cloned into the linearized pGADT7 vector. The Y2HGold yeast strain was transformed with recombinant plasmids, using the small-scale transformation protocol.

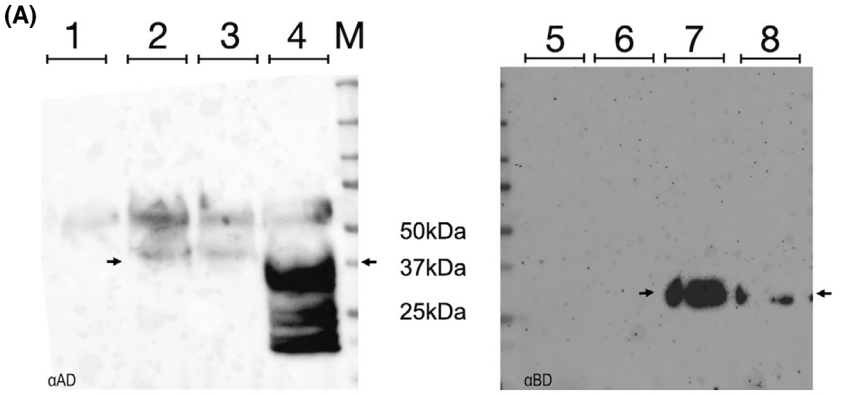

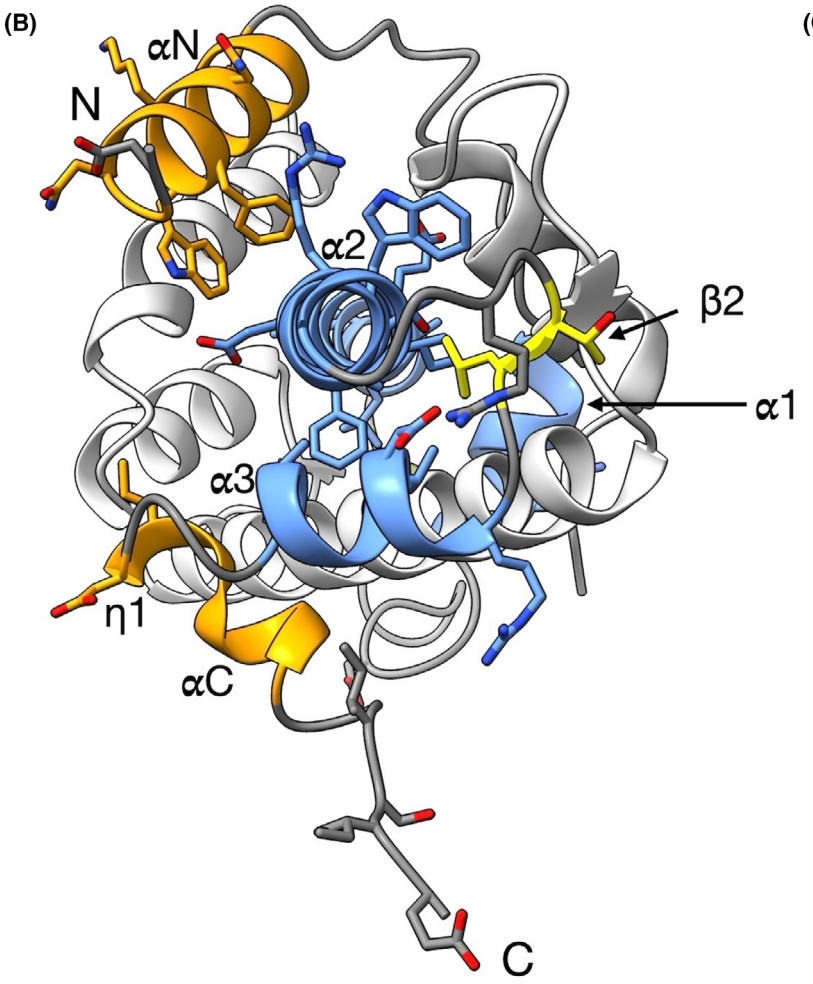

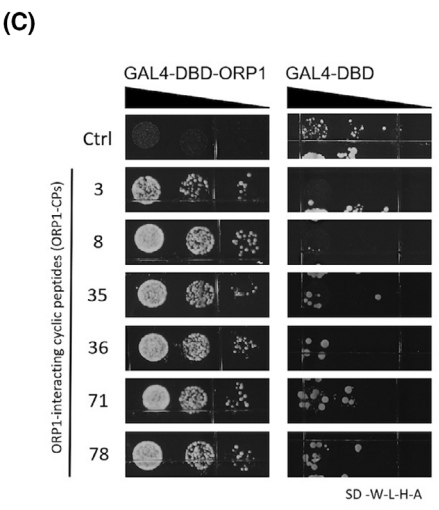

#3 1-IMSSLRWW-8
#8 IWYGGGWW
#35 CRRIASIY
#36 ALSQFIIK
#71 MMFAILNV
#78 RRTYSVLL

Color

Fig. 6. Yeast two-hybrid assay for the analysis of the oocyst rupture protein dimer interface and the identification of six cyclic peptides that interact with ORP1^{HFD}. (A) Expression of GAL4-AD (αAD) in Y2HGold yeast strain transformed with pGADT7-ORP2^{HFD} (2), pGBKT7-ORP1^{HFD} (3), pGADT7-ORP2^{HFD} + pGBKT7-ORP1^{HFD} (4); Right panel: expression of GAL4 DNA-BD (αBD) in Y2HGold yeast strain transformed with pGADT7-ORP2^{HFD} (6), pGBKT7-ORP1^{HFD} (7), and pGADT7-ORP2^{HFD} + pGBKT7-ORP1^{HFD} (8). 1 and 5 illustrate nontransformed Y2HGold controls (Ctrl). The molecular weight (MW) markers (M) are shown in kDa. Arrows indicate the expected MW of the fusion proteins. The band observed in Lane 3 may correspond to a nonspecific signal. Histone-fold domain is abbreviated as HFD. (B) Invariant residues of ORP2^{HFD} located on the crystal structure. Side view of the crystal structure of the HFD dimer with ORP1^{HFD} shown in light gray ribbons and ORP1^{HFD} colored as in Fig. 2 with α-helices and β-strands in blue and yellow, respectively, and α-helices that are extra with respect to the canonical HFD, in orange. Visible secondary structure elements in ORP2^{HFD} are labeled. The 38 amino acid residues that are conserved in all mutant clones analyzed are shown as sticks and colored according to the secondary structure element in which they are found, with heteroatom coloring. Residues 1–4 are not shown as they are absent in the crystal structure due to flexibility at the N terminus. This figure was generated using ChimeraX version 1.8 [21]. (C) Yeast two-hybrid-based identification of cyclic peptides (CPs) that interact with ORP1^{HFD}. Diploid yeast cells expressing six different GAL4AD-ORP1^{HFD}-CPs (numbered 3, 8, 35, 36, 71 and 78) and either the GAL4-DBD-ORP1^{HFD} chimera or the GAL4-DBD protein, were assayed on selective media to verify yeast growth by activation of His3 and Ade2 reporter genes. After normalization to an optical density at 600 nm (OD^{600nm}) of 0.5, yeast cultures were serially diluted and spotted on selective media. The sequences of the six cyclic peptides are shown on the right.

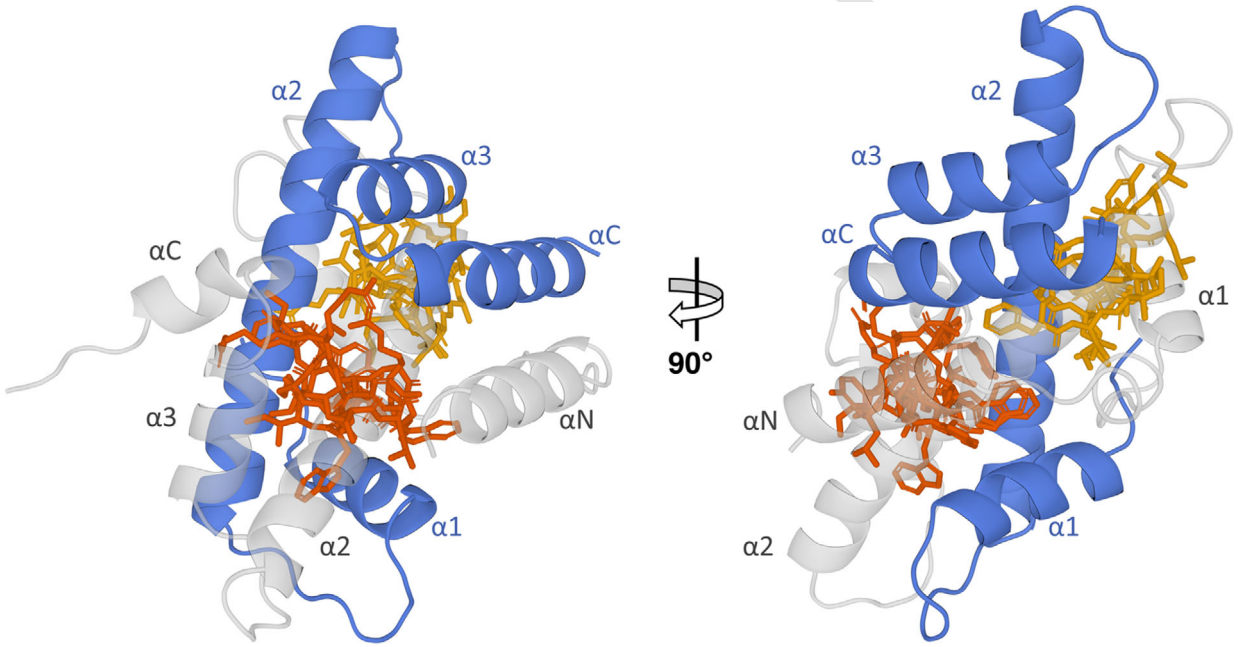

Color

Fig. 7. *In silico* binding poses of selected cyclic peptides at the ORP1/ORP2^{HFD} dimerization interface. The left panel shows the ORP1/2 histone-fold domain (HFD) heterodimer, with ORP1^{HFD} in solid, blue cartoon format and ORP2^{HFD} in transparent gray cartoon format. Superposition of the most representative docking poses of the six selected cyclic peptides: CP3, CP8, and CP35 (orange sticks; C site); CP36, CP71, and CP78 (yellow sticks; N site), is shown. The docking poses reflect the binding surface overlap with the ORP1/2^{HFD} interface, mimicking interactions observed in the native heterodimer. For clarity, hydrogen atoms are omitted. The right panel shows the same complex rotated 90° around the y-axis. This figure was generated using PyMOL open-source, version 2.6 (Schrödinger, LLC.).

PCR was performed on colonies using GoTaq Polymerase (Promega) and 5X GoTaq Reaction Buffer (Promega) (5 min denaturation at 95 °C, 35 cycles of denaturation at 95 °C for 15 s, annealing at 60 °C for 30 s, and elongation at 72 °C for 30 s and a final elongation step at 72 °C for 5 min). Colony-PCR products were sequenced with sequence-specific primers by Eurofins Genomics (Germany) and aligned to the ORP2^{HFD} transcript.

Western blotting

Western blotting was performed to confirm that the interacting proteins were effectively the two HFDs of ORP1 and ORP2. Proteins were extracted from transformed and co-transformed yeasts, following the Urea/SDS Extraction Method, as described in the Yeast Protocols Handbook.

Proteins were separated on mini-PROTEAN TGX Stain-Free Precast Gels 4–20% (Bio-Rad) gels and transferred to Trans-Blot Turbo Transfer pack PVDF (Bio-Rad) mini membranes. Membranes were blocked in EveryBlot Blocking Buffer (Bio-Rad) for 5 min and then incubated overnight at 4 °C with primary antibodies. After washing with 0.1% (*v*/*v*) Tween in 1X PBS, membranes were incubated with HRP-conjugated secondary antibodies (1:5000,

Table 3. Docking summary of the six CPs to ORP1^{HFD}.

Cyclic peptide	Sequence (residues 1–8)	Docking score	CP residue	ORP2^{HFD} residues and secondary structure elements
#3	IMSSLRWW	−6.016	I1	α2: F66; η1: I100, F101; αC: L104
			M2	α3: V91, A95
			S3	α2: T71
			L5	αN: F9
			R6	loop between α3/η1: R97, K98
			W7	α2: I67, M68
			W8	α2: I67, M68
#8	IWYGGGWW	−3.397	I1	α3: V91, I92
			W2	η1: F101; αC: F103, L104; C-ter L107
			Y3	α2: Y73
			W7	α2: I67
			W8	α2: W75
#35	CRRIASIY	−6.413	C1	α2: F66; αC: F103, L104
			R2	α3: R88
			R3	loop between α3/η1: R97, K98
			I4	α2: F70; α3: V91, I92, A93, A94
			A5	α2: F70; α3: V91, I92, A93, A94
			S6	α2: T71
			I7	α2: F70; α3: V91, I92, A93, A94
#36	ALSQFIIK	−4.808	A1	α2: A60
			L2	α2: L59
			F5	α2: L65
			I6	α1: I32; α2: V57
			I7	α1: I32; α2: V57
			K8	α1: K36; loop between α1/α2: K40, K44
#71	MMFAILNV	−4.370	M1	α1: M39
			M2	α2: V57
			F3	α2: L58, L65
			A4	α2: A53
			I5	β1: I51
			L6	β1: I51
			V8	α1: I35, I38
#78	RRTYSVLL	−4.523	R1	α1: R34
			R2	loop between α1/α2: K40, K44
			T3	loop between αN/α1: K40, K44, T27
			V6	α2: L59
			L7	loop between αN/α1: L30; α1: I35; α2: A60
			L8	loop between αN/α1: L30; α1: I35; α2: A60

The sequences of the six CPs are shown, together with their docking scores. For each amino acid residue of each CP, the corresponding ORP2^{HFD} residue with whom it aligns is reported, together with the secondary structure element in which the ORP2^{HFD} residue is housed. The atoms involved in the hydrogen bond are shown in parenthesis, together with the bond lengths in Å. Interface residues were identified using chains C (ORP1^{HFD}) and D (ORP2^{HFD}) and the PDBePISA server [27].

Color

Fig. 8. Comparison of the in silico docked poses of cyclic peptides CP3, CP8, and CP35, superposed with ORP2^{HFD} bound to ORP1^{HFD}. In all panels, the histone-fold domain (HFD) of ORP1 is shown in solid blue cartoon format. Left panels (A–C) show the docking poses of cyclic peptides CP3 (A), CP8 (B), and CP35 (C), with peptide residues shown in sticks (carbon atoms in gray, nitrogen atoms in blue, and oxygen atoms in red). Right panels show the corresponding binding region of ORP2^{HFD} (transparent gray cartoon format) from the crystal structure, with ORP2^{HFD} residues analogous to those in the peptide models also rendered in sticks using the same color scheme. Hydrogen atoms are omitted for clarity. This figure was generated using PyMOL open-source, version 2.6 (Schrödinger, LLC.).

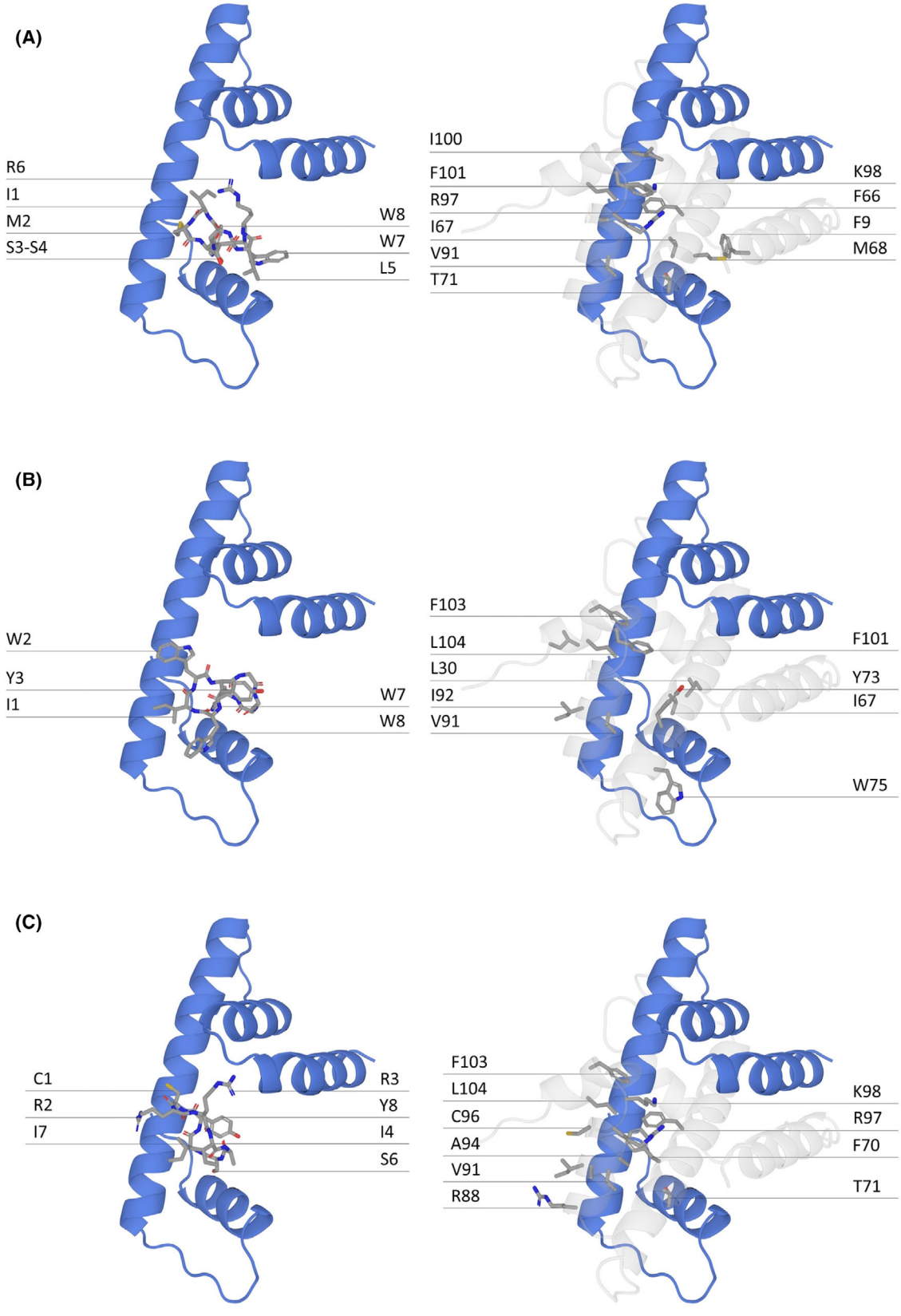

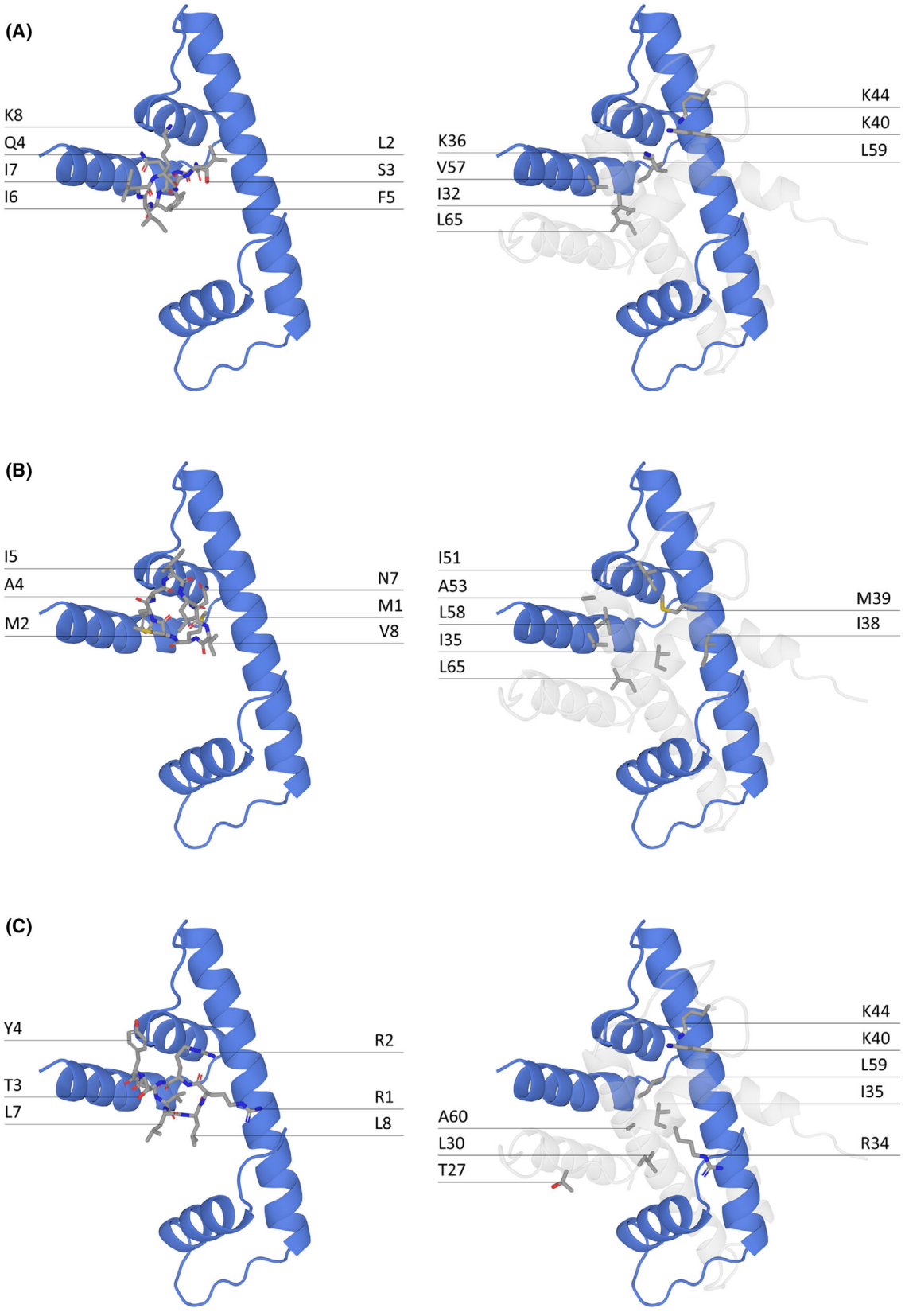

Color

Fig. 9. Comparison of the in silico docked poses of cyclic peptides CP36, CP71, and CP78, with ORP2^{HFD} bound to ORP1^{HFD}. In all panels, the histone-fold domain (HFD) of ORP1 is shown in solid blue cartoon format. Left panels (A–C) show the docking poses of cyclic peptides CP36 (A), CP71 (B), and CP78 (C), with peptide residues shown in sticks (carbon atoms in gray, nitrogen in blue, and oxygen in red). Right panels show the corresponding binding region of ORP2^{HFD} (transparent gray cartoon) from the crystal structure, with ORP2^{HFD} residues analogous to those in the peptide models also rendered in sticks using the same color scheme. Hydrogen atoms are omitted for clarity. This figure was generated using PyMOL open-source, version 2.6 (Schrödinger, LLC.).

```
ORP1HFD 768  MNKNDNETLLPIANISRIMKRILPAKAKVAKESKDIIREYVTEFIQFLTSEASDRCLNEKRKTINGEDILFSMEKLGF
hNF-YB  48   MSFREQDIYLPIANVARIMKNAIPQTGKIAKDAKECVQECVSEFISFITSEASERCHQEKRKTINGEDILFAMSTLGF
             *. .:::  *****::****. :* ..*:**::*: ::* *:***.*:*****:** :*************:*..***
ORP1HFD      NDYVEPLSEYLNKWKQ 860
hNF-YB       DSYVEPLKLYLQKFRE 141
             :.*****. **:*:::
```

Color

Fig. 10. Conservation of the hydrophobic residues at the dimer interface of ORP1^{HFD} and human NF-YB. Amino acid sequence alignment made between the histone-fold domain (HFD) of ORP1 and human NF-YB, using ClustalOmega [26]. The conservation of buried, solvent inaccessible hydrophobic interface residues in NF-YB with solvation energy values >0.5 kcal·mol^{-1} as reported in Chaves *et al.* [29] is shown with identical (blue), conservative (green), and nonconservative (orange) residues colored accordingly and highlighted in bold font. Overall conservation of the aligned sequences is 56.38%.

10

Santa Cruz, sc-2004) for 1 h at room temperature. After washing with PBS, proteins were detected using Clarity Western ECL Substrate (Bio-Rad) and the ChemiDoc imaging system (Bio-Rad).

Primary antibodies used were the rabbit, anti-GAL4 AD antibody (0.5 μg·mL^{-1}, Sigma-Aldrich) and mouse, anti-GAL4 DBD monoclonal antibody (0.5 mg·mL^{-1}, Clontech), while Goat anti-Rabbit IgG (H + L) Secondary Antibody, HRP (1:30000; Thermo Fisher Scientific) and Goat anti-Mouse IgG (H + L) Secondary Antibody, HRP (1:10000; Thermo Fisher Scientific) were used as secondary antibodies.

Plasmids, yeast strains and CYCLIC library mating-based Y2H screening

GAL4-DBD-ORP1^{HFD} was expressed using the pGBKT7-GW plasmid, cloning ORP1^{HFD} at the C terminus of the GAL4-DBD, before transformation into the Y187 (MATα, ura3-52, his3-200, ade2-101, trp1-901, leu2-3, 112, gal4Δ, met–, gal80Δ, URA3::GAL1UAS-GAL1TATA-lacZ) yeast strain (Clontech). The CYCLIC library was constructed, as previously described [32]. To identify CPs (ORP1^{HFD}-CPs) that interact with ORP1^{HFD}-DBD, Y187 yeast cells, transformed with pGBKT7-ORP1^{HFD} vector, were mated with CYCLIC-expressing AH109 yeast cells, according to Takara Bio USA (PT4084-1) guidelines. Mated cells were plated on Synthetic Dropout (SD) media lacking tryptophan, leucine, histidine, and adenine (-W-L-H-A) and incubated at 28 °C for 10 days. Colonies grown on selective media were collected and sampled for yeast colony PCR. To identify peptide-encoding sequences, amplicons were sequenced by Eurofins Genomics (Germany).

ORP1^{HFD}-CP interaction validation

To ensure that identified CPs effectively interact with ORP1^{HFD} or the GAL4-DBD scaffold, ORP1^{HFD}-CPs were amplified by exploiting classical PCR procedures and amplicons were used to transform AH109 yeast cells, together with the linearized version of pGADT7-SspIntein, as previously described [32]. AH109 yeast cells harboring the pGADT7-SspIntein-ORP1^{HFD}-CP expression vector were then mated with Y187 yeast cells transformed with the pGBKT7-GW plasmid. The interaction strengths between isolated ORP1^{HFD}-CPs and GAL4-DBD or ORP1^{HFD}-CPs and GAL4-DBD-ORP1^{HFD} were evaluated by culturing diploid cells in liquid medium, normalizing the Optical Density at 600 nm (OD^{600nm}) to 0.5, and spotting serial dilutions onto SD-W-L (control) and SD-W-L-H-A. Yeast cells that grew in the presence of GAL4-DBD-ORP1^{HFD} but not in the presence of GAL4-DBD were designated as ORP1^{HFD} interactors and kept for further analysis.

Recombinant production of the ORP1/2^{HFD} heterodimer

The cDNA coding for the C-terminal, NF-YB-like HFD (amino acid residues 768–860) of ORP1 (PlasmoDB code: PBANKA_0902500) was cloned in-frame with a N-terminal histidine tag into the pET-15b expression vector (Novagen) via *NdeI* and *XhoI* restriction sites. The cDNA coding for residues 1 to 111 of the N-terminal, NF-YC-like HFD of ORP2 (PlasmoDB code: PBANKA_130340) was cloned into the pMCNS expression vector via *NdeI* and *BamHI* restriction sites. BL21(DE3) Star cells (Invitrogen) were

transformed with ORP1^{HFD}-pET-15b, selecting on LB-agar plates supplemented with 100 μg·mL^{-1} ampicillin, and competent cells containing the transformed plasmid were prepared using standard calcium chloride-based methods. The ORP2^{HFD}-pMCNS plasmid was transformed into BL21(DE3) Star cells containing the ORP1^{HFD}-pET-15b plasmid, and double transformants were selected on LB-agar plates supplemented with 100 μg·mL^{-1} ampicillin and 50 μg·mL^{-1} spectinomycin.

The ORP1/2^{HFD} heterodimer was co-expressed in 2X YT medium (1.6% (*w*/*v*) bacto-tryptone, 1.0% (*w*/*v*) yeast extract and 0.5% (*w*/*v*) NaCl) supplemented with 100 μg·mL^{-1} ampicillin and 50 μg·mL^{-1} spectinomycin. Two liters of cultures were routinely grown at 37 °C until optical density values (at 600 nm) of 0.6–0.8 were reached, after which cultures were cooled to 20 °C. Protein expression was induced upon addition of 0.5 mM isopropyl β-D-1-thiogalactopyranoside (IPTG), incubating overnight at 20 °C with shaking (220 rpm). Bacterial cultures were harvested by centrifugation at 11 000 ***g*** and cell pellets were resuspended in Buffer A [20 mM sodium phosphate buffer pH 7.4, 0.5 M NaCl, 10 mM imidazole, 10% (*v*/*v*) glycerol and 1 mM dithiothreitol (DTT)]. Cell lysis was carried out by mechanical rupture at 25 mPa using a Cell Disruptor (Constant Systems Ltd.). Fifty microliters per mL DNases and 10 mM $MgCl_2$ were added to the lysate and incubated on ice for 30 min before sonication for 5 min (cycles of 20 s on, 20 s off). The soluble and insoluble fractions were separated by centrifugation at 34 000 ***g*** for 30 min.

The heterodimer was purified from the soluble fraction by affinity chromatography on a 1 mL HisTrap™ HP column (Cytiva) at a flow rate of 1 mL/min, using a step gradient achieved mixing Buffer A with Buffer B (20 mM sodium phosphate buffer pH 7.4, 0.5 M NaCl, 0.5 M imidazole, 10% (*v*/*v*) glycerol and 1 mM DTT) at 5%, 10%, 20%, 40%, 60%, and 100% Buffer B.

Elution steps were carried out over five column volumes per step. Fractions containing ORP1/2^{HFD} were pooled and concentrated to 1 mL using an Amicon Centrifugal device (Millipore) with a MW cutoff of 10 K, and further purified by SEC on a SepFastTM 11/30 6–600 kDa pg column (Neobiotech), pre-equilibrated in 20 mM Tris–HCl pH 8.0, 0.5 M NaCl, 10% (*v*/*v*) glycerol, and 1 mM DTT, at a flow rate of 0.8 mL·min^{-1}. All chromatographic methods were carried out at 4 °C using the AKTAGo FPLC system (Cytiva).

Crystallization of the ORP1/ORP2 heterodimer

ORP1/2^{HFD} crystals grew at 20 °C, over 7–14 days, in a 400 nL drop prepared by mixing 50% purified ORP1/2^{HFD} (14 mg·mL^{-1}) with an optimized condition of SG1 Shotgun (MiTeGen) condition D6, containing 25% (*w*/*v*) PEG 3500, 0.2 M lithium sulfate ($LiSO_4$) and 0.1 M HEPES pH 7.5. Crystallization trials were performed in 96-well flat-bottomed CrystalQuick™ sitting drop plates (Greiner Bio-One), containing 100 μL reservoir solution, using an Oryx4 crystallization robot (Douglas Instruments). Crystals were cryoprotected in crystallization solution supplemented with 20% (*v*/*v*) ethylene glycol for storage in liquid nitrogen.

X-ray data collection and ORP1/2^{HFD} structure determination

X-ray diffraction data were collected at 3.1 Å resolution at 100 K on the ID23-2 beamline at the European Synchrotron Radiation Facility (ESRF, France). Data were processed and scaled using XDS [36] and Aimless, respectively [37,38]. The ORP1/2^{HFD} structure was solved using MOLREP [39] and the crystal structures of the HFDs of NF-YB2 and NF-YC3 from *Arabidopsis thaliana* (PDB: 6R0M; [29]) as search models for ORP1^{HFD} and ORP2^{HFD}, respectively. The initial molecular replacement solution was found using NF-YB2, followed by NF-YC3, followed by subsequent cycles of manual building in Coot [40] and refinement with phenix.refine [41,42].

Structure validation was performed using Molprobity integrated in Phenix.refine [43]. Data collection and refinement statistics are reported in Table 1.

In silico docking of cyclic peptides to ORP1^{HFD}

The ORP1^{HFD} chain (residues 774–860) was extracted from the crystal structure of the ORP1/2^{HFD} heterodimer to perform the molecular docking procedure. The structure of ORP1^{HFD} was prepared using the Protein Preparation Wizard tool [44] (Schrödinger Maestro suite version 14.2.118, release 2024–4; Schrödinger, LLC, 2024) to resolve steric clashes and other nonfavorable interactions via energy minimization (OPLS [45] force field), to assign the protonation states for ionizable groups at pH 7.4 ± 0.4, and to improve the hydrogen bond network by optimizing the orientation of the hydroxyl and amide moieties.

The models of the CPs CP3, CP8, CP35, CP36, CP71, and CP78 were predicted using the PEPstrMOD webserver, following the standard N-to-C cyclization protocol, which involves a 100 ps molecular dynamics simulation in vacuum [46]. The six CP sequences were, respectively: (i) I1, M2, S3, S4, L5, R6, W7, W8, (ii) I1, W2, Y3, G4, G5, G6, W7, W8, (iii) C1, R2, R3, I4, A5, S6, I7, Y8, (iv) A1, L2, S3, Q4, F5, I6, I7, K8, (v) M1, M2, F3, A4, I5-L6, N7, V8, and (vi) R1, R2, T3, Y4, S5, V6, L7, L8. Explicit CONECT records for all bonds were added using the open-source version of PyMOL (version 2.6; Schrödinger, LLC). Peptide geometries were further optimized using LigPrep from the Schrödinger Maestro suite, with protonation states assigned at pH 7.4 [44]. Amino acid chirality was maintained in accordance with the 3D structures generated by PEPstrMOD [46].

To contain the entire structure of $ORP1^{HFD}$, a docking grid box with an edge length of 76 Å was generated and centered on the geometrical center of the protein. GlideXP with flexible ligand sampling was used to perform the blind docking of each CP to $ORP1^{HFD}$ [44]. A second round of docking was performed enabling the Prime macrocycle sampling to extend the number of conformers and poses [47].

All poses were visually inspected using PyMOL and Schrödinger 2D Sketcher (Schrödinger, LLC). In addition to the docking score, the similarity to the binding mode of $ORP2^{HFD}$ to $ORP1^{HFD}$ observed in the solved crystal structure was used as a criterion for pose selection to identify the most promising binding model for each CP.

Acknowledgements

We acknowledge the European Synchrotron Radiation Facility for provision of synchrotron radiation facilities, and we would like to thank the ESRF staff for assistance in using beamline ID23-2. This project was funded by Hellenic Foundation for Research and Innovation HFRI – 2nd call for post doc ELIDEK contract number 29168-22102020 awarded to Chiara Currà. LJG gratefully acknowledges Università degli Studi di Milano 'Linea 2' funding. MV and AB were funded by Università degli Studi di Milano 'Grandi Sfide di Ateneo (GSA)'. FB acknowledges the Next Generation EU project PRIN 2022 (20225X2FS5 and CUP B53D23015140006). SM and CB received funding from the EU Horizon 2020-EU.1.2 Future and Emerging Technologies (FET) open research and innovation action under grant agreement 828940.

Conflict of interest

The authors declare no conflict of interest.

Author contributions

OL, RR, RG, CCu, CP, IS, and LJG carried out cloning protein production. LJG, ADCB, and MN carried out data collection, 3D structure determination, and analysis. CB, MV, PG, and SM planned and performed the Y2H experiments. AK, FB, and CCa planned and performed activities related to *in silico* docking experiments. LJG, CB, MV, FB, SM, MN, and PG wrote the paper.

Data availability statement

The structural data that support these findings are freely available from the protein data bank (https://www.rcsb.org) with accession code PDB: 9RIF. Docking poses are available in the open access Zenodo repository (https://doi.org/10.5281/zenodo.15644502).

References

1 (2024) World malaria report.
2 World Health Organization (2015) Guidelines for the treatment of malaria, 3rd ed World Health Organization, Geneva, Austria.
3 Siden-Kiamos I, Pace T, Klonizakis A, Nardini M, Garcia CRS & Currà C (2018) Identification of plasmodium berghei oocyst rupture protein 2 (ORP2) domains involved in sporozoite egress from the oocyst. *Int J Parasitol* **48**, 1127–1136.
4 Currà C, Gessmann R, Pace T, Picci L, Peruzzi G, Varamogianni-Mamatsi V, Spanos L, Garcia CRS, Spaccapelo R, Ponzi M *et al.* (2016) Release of plasmodium sporozoites requires proteins with histone-fold dimerization domains. *Nat Commun* **7**, 13846.
5 Venugopal K, Hentzschel F, Valkiūnas G & Marti M (2020) Plasmodium asexual growth and sexual development in the haematopoietic niche of the host. *Nat Rev Microbiol* **18**, 177–189.
6 Nakayama K, Kimura Y, Kitahara Y, Soga A, Haraguchi A, Hakozaki J, Sugiyama M, Kusakisako K, Fukumoto S & Ikadai H (2021) Role of plasmodium berghei ookinete surface and oocyst capsule protein, a novel oocyst capsule-associated protein, in ookinete motility. *Parasit Vectors* **14**, 373.
7 Sasaki H, Sekiguchi H, Sugiyama M & Ikadai H (2017) Plasmodium berghei Cap93, a novel oocyst capsule-associated protein, plays a role in sporozoite development. *Parasit Vectors* **10**, 399.
8 Srinivasan P, Fujioka H & Jacobs-Lorena M (2008) PbCap380, a novel oocyst capsule protein, is essential for malaria parasite survival in the mosquito. *Cell Microbiol* **10**, 1304–1312.
9 Nardini M, Gnesutta N, Donati G, Gatta R, Forni C, Fossati A, Vonrhein C, Moras D, Romier C, Bolognesi M *et al.* (2013) Sequence-specific transcription factor NF-Y displays histone-like DNA binding and H2B-like ubiquitination. *Cell* **152**, 132–143.
10 Baxevanis AD & Landsman D (1997) Histone and histone fold sequences and structures: a database. *Nucleic Acids Res* **25**, 272–273.
11 Gnesutta N, Nardini M & Mantovani R (2013) The H2A/H2B-like histone-fold domain proteins at the crossroad between chromatin and different DNA metabolisms. *Transcription* **4**, 114–119.
12 Baxevanis AD, Arents G, Moudrianakis EN & Landsman D (1995) A variety of DNA-binding and multimeric proteins contain the histone fold motif. *Nucleic Acids Res* **23**, 2685–2691.

13 Sondermann H, Soisson SM, Bar-Sagi D & Kuriyan J (2003) Tandem histone folds in the structure of the N-terminal segment of the Ras activator son of Sevenless. *Structure* **11**, 1583–1593.
14 Paton DG, Childs LM, Itoe MA, Holmdahl IE, Buckee CO & Catteruccia F (2019) Exposing anopheles mosquitoes to antimalarials blocks plasmodium parasite transmission. *Nature* **567**, 239–243.
15 Probst AS, Paton DG, Appetecchia F, Bopp S, Adams KL, Rinvee TA, Pou S, Winter R, Du EW, Yahiya S *et al.* (2025) In vivo screen of plasmodium targets for mosquito-based malaria control. *Nature* **643**, 785–793.
16 Njoroge TM, Hamid-Adiamoh M & Duman-Scheel M (2023) Maximizing the potential of attractive targeted sugar baits (ATSBs) for integrated vector management. *Insects* **14**, 585.
17 Kekani LN & Witika BA (2023) Current advances in nanodrug delivery systems for malaria prevention and treatment. *Discov Nano* **18**, 66.
18 Kumar S, Stecher G, Suleski M, Sanderford M, Sharma S & Tamura K (2024) MEGA12: molecular evolutionary genetic analysis version 12 for adaptive and green computing. *Mol Biol Evol* **41**, msae263.
19 Yang Z, Zeng X, Zhao Y & Chen R (2023) AlphaFold2 and its applications in the fields of biology and medicine. *Signal Transduct Target Ther* **8**, 115.
20 Bryant P, Pozzati G, Zhu W, Shenoy A, Kundrotas P & Elofsson A (2022) Predicting the structure of large protein complexes using AlphaFold and Monte Carlo tree search. *Nat Commun* **13**, 6028.
21 Meng EC, Goddard TD, Pettersen EF, Couch GS, Pearson ZJ, Morris JH & Ferrin TE (2023) UCSF ChimeraX : tools for structure building and analysis. *Protein Sci* **32**, e4792.
22 Muralidharan V & Goldberg DE (2013) Asparagine repeats in plasmodium falciparum proteins: good for nothing? *PLoS Pathog* **9**, e1003488.
23 Laskowski RA, Jabłońska J, Pravda L, Vařeková RS & Thornton JM (2018) PDBsum: structural summaries of PDB entries. *Protein Sci* **27**, 129–134.
24 Gnesutta N, Saad D, Chaves-Sanjuan A, Mantovani R & Nardini M (2017) Crystal structure of the *Arabidopsis thaliana* L1L/NF-YC3 histone-fold dimer reveals specificities of the LEC1 family of NF-Y subunits in plants. *Mol Plant* **10**, 645–648.
25 Hortschansky P, Misslinger M, Mörl J, Gsaller F, Bromley MJ, Brakhage AA, Groll M, Haas H & Huber EM (2020) Structural basis of HapEP88L-linked antifungal triazole resistance in aspergillus fumigatus. *Life Sci Alliance* **3**, e202000729.
26 Sievers F, Wilm A, Dineen D, Gibson TJ, Karplus K, Li W, Lopez R, McWilliam H, Remmert M, Söding J *et al.* (2011) Fast, scalable generation of high-quality protein multiple sequence alignments using Clustal omega. *Mol Syst Biol* **7**, 539.
27 Krissinel E (2015) Stock-based detection of protein oligomeric states in jsPISA. *Nucleic Acids Res* **43**, W314–W319.
28 Ye B, Tian W, Wang B & Liang J (2024) CASTpFold: computed atlas of surface topography of the universe of protein folds. *Nucleic Acids Res* **52**, W194–W199.
29 Chaves-Sanjuan A, Gnesutta N, Gobbini A, Martignago D, Bernardini A, Fornara F, Mantovani R & Nardini M (2021) Structural determinants for NF-Y subunit organization and NF-Y/DNA association in plants. *Plant J* **105**, 49–61.
30 Robert X & Gouet P (2014) Deciphering key features in protein structures with the new ENDscript server. *Nucleic Acids Res* **42**, W320–W324.
31 Holm L (2020) Using Dali for protein structure comparison. *Methods Mol Biol* **2112**, 29–42.
32 Rosa S, Tagliani A, Bertaso C, Tadini L, Visentin C, Gourlay LJ, Pricl S, Feni L, Pellegrino S, Pesaresi P *et al.* (2023) The cyclic peptide G4CP2 enables the modulation of galactose metabolism in yeast by interfering with GAL4 transcriptional activity. *Front Mol Biosci* **10**, 1017757.
33 Freedman TS, Sondermann H, Friedland GD, Kortemme T, Bar-Sagi D, Marqusee S & Kuriyan J (2006) A Ras-induced conformational switch in the Ras activator son of sevenless. *Proc Natl Acad Sci USA* **103**, 16692–16697.
34 Akbarian M, Khani A, Eghbalpour S & Uversky VN (2022) Bioactive peptides: synthesis, sources, applications, and proposed mechanisms of action. *Int J Mol Sci* **23**, 1445.
35 Costa L, Sousa E & Fernandes C (2023) Cyclic peptides in pipeline: what future for these great molecules? *Pharmaceuticals* **16**, 996.
36 Kabsch W (2010) XDS research papers. *Acta Crystallogr D Biol Crystallogr* **66**, 125–132.
37 Evans PR & Murshudov GN (2013) How good are my data and what is the resolution? *Acta Crystallogr D Biol Crystallogr* **69**, 1204–1214.
38 Winn MD, Ballard CC, Cowtan KD, Dodson EJ, Emsley P, Evans PR, Keegan RM, Krissinel EB, Leslie AGW, McCoy A *et al.* (2011) Overview of the CCP4 suite and current developments. *Acta Crystallogr D Biol Crystallogr* **67**, 235–242.
39 Vagin A & Teplyakov A (1997) *MOLREP*: an automated program for molecular replacement. *J Appl Cryst* **30**, 1022–1025.
40 Emsley P & Cowtan K (2004) Coot: model-building tools for molecular graphics. *Acta Crystallogr D Biol Crystallogr* **60**, 2126–2132.
41 Afonine PV, Grosse-Kunstleve RW, Echols N, Headd JJ, Moriarty NW, Mustyakimov M, Terwilliger TC, Urzhumtsev A, Zwart PH & Adams PD (2012) Towards automated crystallographic structure

refinement with phenix. *Acta Crystallogr D Biol Crystallogr* **68**, 352–367.
42 Adams PD, Afonine PV, Bunkóczi G, Chen VB, Davis IW, Echols N, Headd JJ, Hung LW, Kapral GJ, Grosse-Kunstleve RW *et al.* (2010) PHENIX: a comprehensive python-based system for macromolecular structure solution. *Acta Crystallogr D Biol Crystallogr* **66**, 213–221.
43 Chen VB, Arendall WB, Headd JJ, Keedy DA, Immormino RM, Kapral GJ, Murray LW, Richardson JS & Richardson DC (2010) MolProbity: all-atom structure validation for macromolecular crystallography. *Acta Crystallogr D Biol Crystallogr* **66**, 12–21.
44 Madhavi Sastry G, Adzhigirey M, Day T, Annabhimoju R & Sherman W (2013) Protein and ligand preparation: parameters, protocols, and influence on virtual screening enrichments. *J Comput Aided Mol Des* **27**, 221–234.
45 Lu C, Wu C, Ghoreishi D, Chen W, Wang L, Damm W, Ross GA, Dahlgren MK, Russell E, Von Bargen CD *et al.* (2021) OPLS4: improving force field accuracy on challenging regimes of chemical space. *J Chem Theory Comput* **17**, 4291–4300.
46 Singh S, Singh H, Tuknait A, Chaudhary K, Singh B, Kumaran S & Raghava GPS (2015) PEPstrMOD: structure prediction of peptides containing natural, non-natural and modified residues. *Biol Direct* **10**, 73.
47 Sindhikara D, Spronk SA, Day T, Borrelli K, Cheney DL & Posy SL (2017) Improving accuracy, diversity, and speed with prime macrocycle conformational sampling. *J Chem Inf Model* **57**, 1881–1894.

Graphical Abstract

The contents of this page will be used as part of the graphical abstract of html only. It will not be published as part of main.

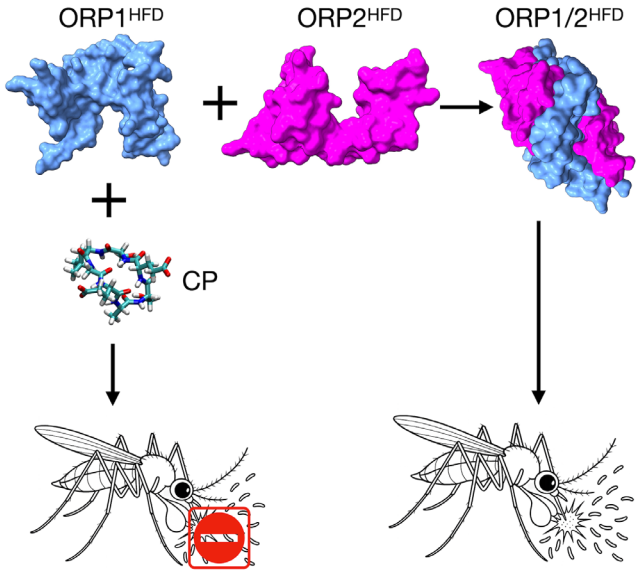

A physical interaction between two oocyst rupture proteins (ORP1 and ORP2) from the oocyst stage of the *Plasmodium* parasite that causes Malaria has been shown to induce oocyst rupture. Rupture occurs in the salivary glands of the mosquito vector host and represents a key event in parasite transmission to humans. We reveal how these proteins interact at a molecular level, and we identify six cyclic peptides as potential oocyst rupture blocking molecules.